Sources of ultrafine particles at a rural Midland site in Switzerland

Lubna Dada[1*], Benjamin T. Brem[1*], Lidia-Marta Amarandi-Netedu[1], Martine Collaud Coen[2], Nikolaos Evangeliou[4], Christoph Hueglin[3], Nora Nowak[1], Robin Modini[1], Martin Steinbacher[3], Martin Gysel-Beer[1]

5   [1]PSI Center for Energy and Environmental Sciences, Villigen PSI, Switzerland

[2]Federal Office of Meteorology and Climatology, MeteoSwiss, Payerne, Switzerland

[3]Laboratory for Air Pollution and Environmental Technology, Swiss Federal Laboratories for Materials Science and Technology (Empa), Dübendorf, Switzerland

[4]Department of Atmospheric and Climate Research (ATMOS), Stiftelsen NILU, Kjeller, Norway

10   *Correspondence to: Lubna Dada (lubna.dada@psi.ch) and Benjamin T. Brem (benjamin.brem@psi.ch)

Abstract

Ultrafine Particles (UFPs, i.e. atmospheric aerosol particles smaller than 100 nm in diameter) are known to be responsible for a series of adverse health effects as they can deposit in humans' bodies. So far, most field

15   campaigns studying the sources of UFPs focused on urban environments. This study investigates the outdoor sources of UFPs at the atmospheric monitoring station in Payerne, which represents a typical rural location in Switzerland. We aim to quantify the primary and secondary fractions of UFPs based on specific measurements between July 2020 and July 2021 complementing a series of operational meteorological, trace gas and in-situ aerosol observations. To distinguish between primary and secondary contributions, we use a method that relies

20   on measuring the non-volatile particles fraction as a proxy for primary particles. We further compare our measurement results to previously established methods. We find that primary particles resulting from traffic and residential wood burning (direct emissions), contribute less than 40% to the total number of UFPs, mostly in the Aitken mode. On the other hand, we observe local NPF events (observed from ~1 nm) evident from the increase of cluster ions and nucleation mode particles concentrations, especially in spring and summer. These events,

25   mediated by sulfuric acid, contribute to increasing the UFPs number concentration, especially in the nucleation mode. Besides NPF, chemical processing of particles emitted from multiple sources (including traffic and residential wood burning) contribute substantially to the nucleation mode particle concentration. Under the present conditions investigated here, we find that secondary processes mediate the increase of UFP concentration to levels equivalent to those in urban locations, affecting both air quality and human health.

1   Introduction

Atmospheric aerosol particles are known for their adverse effects on human health and their impacts on Earth's climate. Among those, a class, namely ultrafine particles (UFPs – diameter < 100 nm), is critical, given the particles' high number concentrations (and surface area) in the atmosphere and their capability to travel deep into the human body and to deposit onto sensitive body parts e.g. brain (Schraufnagel, 2020; Kwon et al., 2020).

35   Therefore, scientists have dedicated a large fraction of research to advance the understanding of the chemical composition, sources and sinks of UFPs (Seinfeld and Pandis, 2012).

UFPs are found to be more abundant close to anthropogenic source locations. Studies conducted in Switzerland have demonstrated the prevalence of UFPs closer to major roads and airports (Meier et al., 2015; Eeftens et al., 2015; Rivas et al., 2020; Bukowiecki et al., 2002), highlighting the contribution of transportation-related

40   emissions as a significant primary source to UFPs. Additionally, Switzerland's proximity to various industrial regions in Europe underscores the role of transboundary pollution in contributing to particulate matter levels (Zotter et al., 2014; FOEN, 2021). Composition-based source apportionment studies are typically done on mass basis for e.g. $PM_{2.5}$ and PM_{10} (particulate matter with diameters less than 2.5 and 10 μm, respectively), with little attention to UFP sources by number (Grange et al., 2021; Trechera et al., 2023; Cai et al., 2024; Chen et al., 2022).

45   Moreover, UFPs can form in the atmosphere from gaseous precursors via chemical processing. One example is new particle formation (NPF). This phenomenon is found to produce the dominant fraction of the total particle number concentration in several environments worldwide (Kerminen et al., 2018). The frequency and intensity of such events depend on various factors including meteorology, the availability of gaseous precursors and the levels of the preexisting particles acting as sinks (Nieminen et al., 2018). Previous studies on NPF have shown that

50   sulfuric acid is the major precursor vapor contributing to the early steps of NPF within the boundary layer, especially in the presence of stabilizing bases such as ammonia and amines. The latter are usually associated with agricultural and husbandry activities, although other sources such as traffic and industry have been reported in polluted megacities (Zhu et al., 2022). Given the abundance of agricultural activities in Switzerland, NPF is expected to be a major process and contributor to UFP. However, NPF field studies in Switzerland have been

55   limited to short-term measurements in high-Alpine environments (at Jungfraujoch, 3580 m a.s.l.) (Bianchi et al., 2016; Manninen et al., 2010) leaving large gaps in our understanding of NPF in rural Switzerland and its contribution to the size-distribution of UFPs.

The contribution of the different sources to the size classes of UFPs can vary depending on the type of the source, location, and time of year. For instance, combustion processes, including vehicle emissions, industrial activities,

60   and biomass burning, typically produce UFPs rich in elemental carbon (soot) and organic compounds in the size range > 10 nm (Cai et al., 2020). Unfiltered diesel -gasoline direct injection- and gas turbine engines are known to emit a significant fraction of UFPs in the smaller size range, down to even few nm, due to their high combustion efficiency (Rönkkö et al., 2017; Maricq et al., 1999; Durdina et al., 2017) but also due to lube oil ash residues and nucleating volatile material (Kittelson et al., 2004). Other sources, natural or anthropogenic, e.g. road-dust

65   resuspension, dust storms, wind-blown pollen and plant debris, can mechanically produce coarse particles that have little to no contribution to UFPs. On the other hand, vapors associated with natural and anthropogenic activities, contribute to secondary aerosol formation and growth, substantially affecting the number size distribution of UFPs (Kulmala et al., 2004; Ma and Birmili, 2015; Sun et al., 2024).

In this study, we delve deeper into the outdoor sources of UFPs observed in Payerne, a typical rural location in

70   Switzerland. We go beyond the traditional characterization of the site based on $PM_{2.5}$ by identifying and quantifying the sources of UFPs, be it primary or secondary. For doing so, we rely on comprehensive long-term particle (and ions) number distribution measurements at the location, starting from ~1 nm particle diameter. To

distinguish between the size-segregated primary and secondary particles, we applied a measurement technique that uses a catalytic stripper. Together with available measurements of meteorological parameters and trace gases, we could characterize (secondary) NPF events at Payerne and quantify their frequency and intensity, as well as the role of agriculture in providing the vapors responsible for their occurrence, and the contribution of such events to the UFPs at the location. Besides NPF, the secondary fraction of particles resulting from the atmospheric processing of available particles (be it primary or secondary) was quantified. The identification and quantification of primary and secondary sources of UFPs, in such a typical rural location in Switzerland, are pivotal steps allowing for targeted interventions to control UFP emissions, reduce pollution and thus exposure risks.

2 Materials and Methods

2.1 Measurement location

The measurements were conducted at MeteoSwiss' aerological station Payerne (46.812 N, 6.942 E, 491 m a.s.l.) in canton of Vaud, Switzerland. The station hosts long-term observations for a variety of programmes like SwissMetNet, ACTRIS (The Aerosol, Clouds and Trace Gases Research Infrastructure), NABEL (National Air Pollution Monitoring Network), BSRN (Baseline Surface Radiation Network), GAW (Global Atmosphere Watch Program) and GRUAN (GCOS Reference Upper-Air Network). The station is about 1 km south-east of the rural town of Payerne and roughly 500 meters north of a major regional road and about 4 kilometers south of the national highway (A-1) and Payerne military airport (Fig. S1). The city of Payerne has a total area of 24.19 km^2 and a population of roughly 10,500 people, in 2023. The Tropospheric Ozone Assessment Report Activity categorized the Payerne station as a rural site, based on satellite-retrieved NO_2 column concentrations, the surrounding population density, and the intensity of nighttime lights (Schultz et al., 2017). The Payerne site is also part of the European Monitoring and Evaluation Programme (EMEP) (Tørseth et al., 2023). EMEP's siting criteria require large spatial representativeness meaning that monitoring sites are only little influenced by local processes such as emissions, sinks, or topographic features, etc. (EMEP/CCC, 2001). Consequently, lower aerosol mass concentration compared to the other urban and suburban stations of the NABEL network are observed. As for the site itself, shown from the land use map (Fig. S1B), croplands and grasslands surround the measurement station resulting in contributions from agricultural practices. The station is located slightly uphill and elevated (~40 m) above the adjacent emission sources (city, roads and airport).

2.2 Measurement instrumentation and details

A summary of all instruments used for this study are shown in Table S1. The investigated period covers the time between July 2020 and July 2021 when the routinely performed monitoring activities were complemented by additional aerosol number size distribution and NPF analyses. All data shown below are reported in Central European Time (CET; i.e. UTC+1).

2.2.1 Meteorology and Boundary Layer Height

In-situ global radiation, temperature, precipitation, wind speed and wind direction data were obtained from the SwissMetNet (https://opendata.swiss/de/dataset/automatische-meteorologische-bodenmessstationen, last access 26.09.2024), the automatic measurement network of MeteoSwiss. Temperature and wind speed profiles originates

from the EMER-Met (Emergency Response Meteorology) network. The mixing layer height (MLH) was estimated from the temperature profile measured by the MicroWave Radiometer (MWR, HATPRO-G2 produced by RPG Radiometer Physics Gmbh) and the wind speed profiles measured by the Radar Wind Profiler (WP, PCL1300 produced by Degreane) by the bulk Richardson method that takes potential energy and wind shear into account (Collaud Coen et al., 2014). During nighttime, when the MLH is lower than the first level of measurement of the MWR, the data are unavailable resulting in a slight overestimation of the average MLH.

2.2.2 Trace gases

A suite of trace gases such as ozone (O_3), nitrogen dioxide (NO_2), sulfur dioxide (SO_2) and ammonia (NH_3) were measured at Payerne (Bundesamt für Umwelt, 2023). For the period of interest here, surface O_3 was monitored by UV absorption photometry (Thermo Scientific 49i), NO_2 was measured by chemiluminescence (Thermo Scientific 42i TL), SO_2 was measured by UV fluorescence (Thermo Scientific 43i TLE), and NH_3 was detected by Cavity Ringdown Spectroscopy (Picarro Inc., G2103). Details about the measurement procedures for the individual species can be found in the NABEL's technical report (EMPA & BAFU, 2023). The terminology 'concentration' used throughout the manuscript refers to the mixing ratio of the trace gases, in ppb, unless specified otherwise.

2.2.3 Particle number size distribution measurements

The particle number size distribution between 2.5 and 470 nm was measured using a Neutral Cluster and Air Ion Spectrometer (NAIS) and Scanning Mobility Particle Sizer (SMPS) placed in parallel. The NAIS measured the particle number size distributions between 2.5 and 42 nm, whereas the SMPS (TSI3034) measured the size range between 10 and 487 nm, in 3-minute time resolution. A condensation particle counter was also deployed, the CPC (CPC 3022) with a lower cut-of diameter ($D_{50\%}$) of 7 nm, with 1 second time resolution. In addition, the particle number size distribution of naturally charged positive and negative ions in the size range of 0.8 – 42 nm were measured using the NAIS.

The SMPS data were corrected for multiply charged particles and particle losses within the instrument and inlet lines (Liscinsky and Hollick, 2010; Yook and Pui, 2005). The NAIS is expected to overestimate the particle concentration by up to a factor of 10, with charging being the major source of uncertainty (Kangasluoma et al., 2020; Gagne et al., 2011). Here, the ratio of SMPS to NAIS in the overlapping size range 20 – 30 nm (highest detection efficiency size range for both instruments) was used to derive a correction factor for the NAIS. The NAIS was found to overestimate the concentration by a factor 3.5, which is the factor used to correct the NAIS concentration before combining the data with the SMPS. An example, during an NPF event and another during a nonevent day, are shown in Fig. S2, respectively. The overlapping size-cut was defined to be 25 nm until May 31st and 12 nm after that due to unreliable data from the NAIS for diameters >12 nm resulting from a dirty malfunctioning electrometer. NAIS data were available between 09 October 2020 and 31 July 2021. Please refer to table S1 for data availability.

We define four classes of particles based on the combined size distribution measurements. Ultrafine particles are defined as all particles with diameters less than 100 nm, Aitken mode particles have diameters between 25 and

145 100 nm, nucleation mode particles have diameters between 2.5 and 25 nm, and cluster ions have diameters between 1.5 and 3 nm.

2.2.4 Particle number size distribution of non-volatile particles

An additional SMPS (TSI3938) was placed behind a catalytic stripper to measure the non-volatile particles in the size range 3 – 110 nm, in 1 minute time resolution. The catalytic stripper (CS015, Catalytic Instruments GmbH)
150 has an operating gas temperature of 350°C which evaporates the volatile particles allowing the non-volatile fraction to be measured by the SMPS. The catalytic stripper was combined with an automated switching system that alternated, automatically, between total and non-volatile particles measurements every 5 minutes. Non-volatile size-distribution data were available between 19 December 2020 and 03 March 2021. Please refer to table S1 for data availability.

155 ### 2.2.5 Equivalent black carbon

Equivalent Black Carbon concentrations were determined from an aethalometer (Model AE31; Magee Scientific Inc.) measuring at seven wavelengths (370, 470, 520, 590, 660, 880, and 950 nm), with a time resolution of 5 minutes. In this study, we use the 880 nm channel, hereafter, referred to as Black Carbon (BC). Data processing followed GAW/ACTRIS recommendations and included corrections for filter loading and multi-scattering effects
160 (Zanatta et al., 2016).

3 Data analysis

3.1 Brightness parameter

The brightness parameter (*B*) is a parameter used to *estimate* the degree of cloudiness at a certain location. It is defined by the fraction of the total solar radiation reaching the measurement site where the only blockage
165 considered is existing clouds (Dada et al., 2017; Sánchez et al., 2012). Hence, the ratio of the measured global radiation to the theoretical maximum solar radiation at the top of the atmosphere are used to calculate *B*:

$$B = \frac{Global\ Radiation}{Theoretical\ Maximum} \tag{1}$$

The larger the *B* value, the less clouds are in the sky and more radiation arrives to ground level. A complete cloud cover is defined as *B* < 0.3 and clear sky is defined as *B* > 0.7.

170 ### 3.2 BC concentration as a tracer for primary particles

For determining the relative contributions of primary and secondary particles to the size segregated particle concentrations over the full year of measurements, we use the empirical method suggested by Rodríguez and Cuevas (2007) and modified by Kulmala et al. (2016) that uses BC mass concentration as a tracer for primary particles. Using this method, the concentration of primary particles, N_1, is estimated from measured BC
175 concentrations using the following equation:

$$N_1 = S_1 \times BC \tag{2}$$

Here, S_1 is the semi-empirical scaling factor derived from the particle concentration to BC ratio. S_1 is determined as the minimal N-to-BC ratio, or a low percentile (e.g. 0.1%, 1% or 5%) of all observed N-to-BC ratios. The concentration of secondary particles, N_2, is obtained from the difference of total particle number concentration (*N*) and the primary fraction (N_1):

$$N_2 = N - N_1 \qquad\qquad (3)$$

The fractions of primary and secondary ultrafine and accumulation mode particles derived from this method were compared to the corresponding fractions determined by the non-volatile particle measurement method described in section 2.2.4 over the 3-month period when the catalytic stripper (section 2.2.4) was deployed.

3.3   New particle formation events classification

Days in Payerne were classified into NPF event or nonevent days depending on the evolution of their particle number size distributions. Here, we followed the traditional method introduced by Dal Maso et al. (2005), and modified later to include regional and transported events by Dada et al. (2018) based on the size distributions below 3 nm. We, however, tailored the method to fit our measurement location better, which is subject to traffic emissions, as the previous two methods were developed for the boreal forest environment. Our classification scheme is shown in Fig. S3. In brief, NPF events are recognized by the appearance of particles in the nucleation mode exhibiting signs of growth. Five classes were defined in our study. *Local events* (1) are those observed to start in the sub-3 nm range (i.e., hourly-averaged concentration of $1.5 - 3$ nm ions > 20 cm^{-3}), while *transported events* (2) are those observed starting at larger sizes (i.e., hourly-averaged concentration of $7 - 25$ nm particles > 3000 cm^{-3}) indicating their transportation to the measurement location (horizontally or vertically). Alternatively, some events are observed to start at small sizes (sub-3 nm) but fail to grow past a couple of nanometers. These events are referred to as *bumps* (3). Days during which none of the aforementioned phenomena were observed are considered *nonevent days* (4). Days which are affected by rain (rain rate > 0 mm) or high traffic influence (determined as NO_2 concentrations > 3 ppb) are classified as *undefined days* (5), as an NPF event cannot be visually inferred.

3.4   Condensation and Coagulation sinks

Condensation sink, CS, is the rate at which gaseous precursors are lost to pre-existing particles. Here, the CS for sulfuric acid was calculated using the SMPS data following the method described in Kulmala et al. (2001) and Kulmala et al. (2012). The coagulation sink (CoagS) describes the rate at which freshly formed particles are lost to pre-existing particles. In this study, the CoagS was calculated using the combined size distribution (see section 2.2.3) following the method described in Kulmala et al. (2001) and was used an input for the calculation of particle formation rates, section 3.6.

3.5   Particle growth rates

Particle apparent growth rates (GR) were calculated using the 50% appearance time method from the positive ions number size distribution data measured by the NAIS (Dada et al., 2020b). The method relies on the determining the times when the concentration in each size bin reaches 50% of the maximum concentration. In this study, the

GR for the size classes 1.5 – 3 nm, 3 – 7 nm and 7 – 15 nm were determined. The growth rates were also used in the formation rates' calculation in the next section.

3.6 Particle formation rates

215   Particle formation rates at 2.5 nm ($J_{2.5}$) were calculated using the balance equation described in Kulmala et al. (2012) where the change in concentration of particles within a certain size bin (here 2.5 – 7 nm) depends on the particle sources (NPF) and the available sinks; here coagulation sink (CoagS$_{Dp}$) and growth out of the size bin.

$$J_{Dp} = \frac{dN_{Dp}}{dt} + CoagS_{Dp} \cdot N_{Dp} + \frac{GR}{\Delta_{Dp}} \cdot N_{Dp} \tag{4}$$

220

Dp represents the lower diameter of the bin (here 2.5 nm), N_{Dp} is the particle number concentration inside the size bin (2.5 - 7 nm), and GR is the growth rate of particles out of the bin (GR$_7$). ΔDp is the difference between the upper and lower ends of the size bin of interest (here ΔDp =4.5 nm). However, during the events for which a GR could not be calculated, given the change of air mass or the interruption of the growth, or during nonevent days,

225   we used a median growth rate of all the events in the same month to estimate the formation rate. Such an estimation is valid given the similarity in particle GR regardless of the occurrence or intensity of NPF, see also Kulmala et al. (2022).

3.7 Extrapolation of particle formation rates

The particle formation rates at $J_{1.5}$ were extrapolated from $J_{2.5}$ following the analytical formula derived by

230   Kerminen and Kulmala (2002):

$$J_{dp_1} = J_{dp_2} \times \exp\left(-\gamma \frac{CS'}{GR_{dp_2 - dp_1}} \left(\frac{1}{dp_2} - \frac{1}{dp_1}\right)\right) \tag{5}$$

where γ is a coefficient with an approximate value of 0.23 m³ nm² s⁻¹ derived from the ratio between GR and CS′ (Eq. 11 and 13 in Kerminen and Kulmala (2002)). Here dp_1 = 1.5 nm, dp_2 = 2.5 and GR between 1.5 and 3 nm is calculated as GR$_{2.5-7}$ divided by 3 (Kulmala et al., 2013). In addition, CS'=4πD/CS; where CS is the

235   condensation sink, described in section 3.4, and D is the sulfuric acid diffusion coefficient.

We find that the exponent term in our case, where CS$_{average}$ = 0.005 and GR$_{2.5-7\ nm(average)}$ = 3.4 nm/h, is 1.0002, and hence expect that $J_{2.5} \sim J_{1.5}$. In Fig. S4, we show a histogram of the ratio of $J_{1.5}$ to $J_{2.5}$ in 5 minutes time steps and find that the ratio falls between 1 and 1.04, concentrated at 1. Therefore, for the rest of the analysis, $J_{1.5}$ is approximated as measured $J_{2.5.}$

240   **3.8   Sulfuric acid proxy (H₂SO₄,proxy)**

The sulfuric acid proxy was calculated based on the sources and sinks of sulfuric acid in a rural environment setting as discussed in Dada et al. (2020). The main source of H₂SO₄ in the gas phase is the oxidation of SO₂ by the hydroxyl radical (OH) while its sinks are mainly the loss of H₂SO₄ onto pre-existing particles, CS, as well as its loss to cluster/particle formation (Dada et al., 2020). Since OH concentrations were not measured due to

245   instrument limitations, global radiation was used as an OH proxy (Dada et al., 2020; Petäjä et al., 2009). The
       equation is as follows:

$$[H_2SO_4] = -\frac{CS}{2k_3} + \sqrt{\left(\frac{CS}{2k_3}\right)^2 + \frac{[SO_2]}{k_3}(k_1 \times Global\ Radiation)} \tag{6}$$

where k_1 and k_3 are coefficients specific for rural locations, represent the H_2SO_4 production from SO_2 in the
presence of radiation and loss of H_2SO_4 to clustering, and are 0.92 x 10^{-8} $m^2W^{-1}s^{-1}$ and 2.21 x 10^{-9} cm^3s^{-1},

250   respectively (Dada et al., 2020).

3.9   Contribution of NPF to UFP

The contribution of NPF events to UFP concentration ($\bar{N}_{NPF}$) could be calculated as suggested by Sun et al.
(2024):

$$\bar{N}_{NPF} = \frac{\bar{N}_{NPF-HR} \times n_{NPF-HR} + \bar{N}_{NPF-LR} \times n_{NPF-LR}}{n_{NPF-HR} + n_{NPF-LR} + n_{NON-HR} + n_{NON-LR}} \tag{7}$$

255   where $\bar{N}_{NPF-HR}(\bar{N}_{NPF-LR})$ are the integrated diurnal of the difference between UFP concentration between events
       and nonevents under high radiation (low radiation). n_{NPF-HR} (n_{NPF-LR}) and n_{NON-HR} (n_{NON-LR}) are the number of high-
       radiation (low-radiation) days with and without NPF events, respectively. We note that similar to Sun et al. (2024),
       days are separated into high-solar-radiation and low-solar-radiation days by a threshold of daily average global
       radiation of 100 W m^{-2}.

260   ## 4   Results

4.1   Characterization of Payerne site

4.1.1   Meteorology

Payerne, a typical rural location in Swiss midlands, experiences a temperate climate characterized by distinct
seasonal variations in terms of temperature and precipitation (Fig. S5 – S6). Winter, between December and

265   February, is relatively dry compared to spring, between March and May, which witnesses increased precipitation
       and the emergence of blooming vegetation. Summer, spanning from June to August, is occasionally interrupted
       by short bursts of heavy rain from thunderstorms occurring mostly in the afternoon. Autumn, covering September
       to November experiences increased precipitation, as temperatures cool. Solar radiation and cloudiness levels
       follow the seasonal pattern, with higher levels in summer and lower levels in winter and autumn (Fig. S5 – S6).

270   #### 4.1.2   Variability of trace gases

The diurnal cycles (Fig. 1) and the time series (Fig. S7) of the trace gases with dominant sources from fossil fuel
combustion, traffic, residential wood burning and industrial activities (NO_2, SO_2) reflect the rural conditions at
Payerne. Concentrations are lower compared to ones observed at urban locations within the Swiss national
network (Bundesamt für Umwelt, 2023). However, short-term variability in the time series and the diurnal patterns

275   indicate some influence from local to regional processes.

Ozone concentrations are influenced by various factors, such as sunlight, temperature, and concentrations of other pollutants such as volatile organic compounds and NO_2, with generally higher levels observed in spring and summer. For the gaseous pollutants NO_2 and SO_2, it is common for rural areas to have lower concentrations compared to urban environments (EEA, 2023), yet, their concentration can be influenced by various factors,

280   including agricultural practices, traffic, local industrial activities, and long-range transport (Jion et al., 2023; EEA, 2023). Traffic emissions are a major source of NO_2 indicated by the sharp increase of NO_2 during the morning and evening rush hour (Fig. 1, Fig. S7), although other sources such as residential wood burning and use of fertilizers in agriculture could affect the concentration (Jion et al., 2023). NO_2 is observed in higher concentrations on workdays compared to weekends in line with the higher traffic volumes on workdays (Fig. S8B), further

285   confirming the major contribution of traffic emissions to NO_2 concentration in Payerne. The variation between the different seasons is attributed to a shallower boundary layer in winter leading to accumulation of NO_2, compared to better dispersion and vertical mixing during summer (Fig. S9).

Compared to the nitrogen oxides, SO_2 concentrations are influenced by fossil fuel combustion but also long-range transport (Vestreng et al., 2007). Given the proximity of the Payerne airport to our measurement location, we

290   inspected the direct contribution of airport emissions on SO_2 concentrations. We note that Payerne Airport handles an average of 754 civil flights per year, significantly fewer than Zurich Airport, which accommodates around 22,300 flights annually (averages for 2019-2021, Business Aviation Study Switzerland 2022). However, Payerne is the major military airport of Switzerland and has a lot military flight operations. Specifically, we: 1) compared the SO_2 concentrations during workdays and weekends (Fig. S8A), 2) inspected the SO_2 concentration when the

295   wind direction arriving to our measurement station is from the airport (Fig. S8C), 3) studied the SO_2 concentrations during periods of airport holidays (Fig. S8D), and 4) compared the concentrations of SO_2 in Payerne to those at Rigi-Seebodenalp which is approximately 185 km away from Payerne and at an altitude of 1031 m a.s.l. (Fig. S8E). Our results show that while we cannot completely rule out the contribution of the airport activities on SO_2 concentrations observed at Payerne station, the evidence indicates that there is no substantial enhancement of SO_2

300   when airport activities are taking place. For instance, we observe similar levels of SO_2 on workdays and weekends (Fig. S8A), compared to the lower median NO_x concentrations on weekends compared to workdays (Fig. S8B), which are associated with a decrease in traffic intensity. However, we do observe a decrease in the extreme concentrations of SO_2 on weekends compared to workdays (Fig. S8A). Moreover, although wind arriving from the airport direction (NW: $300 - 340 °$) does show elevated SO_2 concentrations, the higher concentrations are not

305   exclusively related to this particular wind direction (Fig. S8C), as Payerne village is also located north-northwest to our measurement site (Fig. S1). Similar to our observation during weekends, SO_2 concentrations do not drop significantly during airport shutdown periods (Fig. S8D), particularly during 2020. Overall, these observations point towards a regional nature of SO_2 emissions. The latter conclusion is further verified by direct comparison between SO_2 concentrations in Payerne and Rigi-Seebodenalp. Similar SO_2 levels are observed at the two sites

310   throughout the year except during winter, when higher concentrations are observed in Payerne due to a shallower mixing layer height (Fig. S9) together with increased local SO_2 emissions from heating sources (EEA, 2023).

On the other hand, ammonia (NH_3) is expected to show higher concentrations in rural environments subject to agricultural practices, such as manure and fertilizers applications (Reche et al., 2022). In Payerne, the highest NH_3 concentrations are observed in spring, with a sharp peak in March when farmers prepare the first fertilization after

315   winter and snow melt (Fig. 1, Fig. S7). In addition, warmer temperatures and longer days promote the release of ammonia (Fig. S10) (Pedersen et al., 2021). In autumn, as harvesting is completed, we observe a decrease in ammonia emissions, although post-harvest practices and the decomposition of crop residues can still contribute to the overall NH_3 concentration. Winter generally witnesses reduced agricultural activity, leading to lower ammonia emissions. The colder temperatures limit volatilization from soil and other surfaces however other

320   sources such as traffic and fossil fuel combustion which emit NH_3 as a byproduct might become more important (Reche et al., 2022).
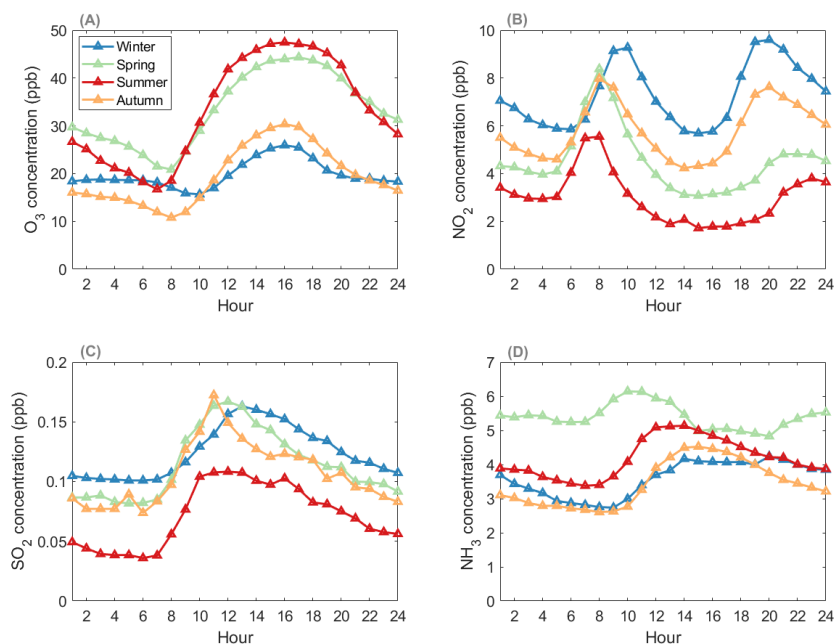
Figure 1 Seasonal diurnal averages of trace gases in Payerne. See Fig. S6 for the full year time series.

325   **4.2   Ultrafine particles at Payerne**

UFP particles in Payerne have multiple sources, some of which are primary (e.g. traffic) or secondary (e.g. NPF). Such sources are expected to have a strong diurnal and day to day variability as we observe a strong variation in the number concentration within each month sometimes exceeding two orders of magnitude (Fig. S11). Regardless, throughout the year, we observe a constant background of ~4000 cm^{-3} UFP (Fig. 2A) along with

330   distinct diurnal patterns on top of this background suggesting considerable contribution from local UFP sources. Our measured UFP concentrations resemble those measured in rural and suburban locations around Europe (Trechera et al., 2023). The Aitken mode contributes around half of the total UFP background and shows very little seasonal variability (Fig. 2C). In contrast, the nucleation mode, which also contributes about half to the UFP background, exhibits a distinct increase during daytime, making it the dominant contributor to total UFP and

335   driving the variability in UFP concentration, especially in spring (62.4%) (Fig. 2B). This observation indicates an important role of nearby emissions and secondary aerosol formation relative to long range transport. During all seasons, the morning and evening peaks are concurrent with rush hours and could be attributed to traffic emissions, visible also in both the nucleation and to a lesser extent in the Aitken modes, in line with previous studies showing the contribution of traffic emissions to these size classes (Zhou et al., 2020; Rönkkö et al., 2017). An additional

340   midday peak in the UFP concentration, driven by nucleation mode particles, is observed in spring and summer indicative of NPF events taking place in warmer seasons. This conclusion is further verified by the increase of cluster ions in these months (Fig. 2D), which are indicative for local NPF, usually more abundant in spring (Dada et al., 2023; Dada et al., 2017) following the onset of vegetation, warmer temperatures and increased solar radiation (Fig. S6). A detailed analysis of NPF events is presented in section 4.4. Although UFP number

345   concentration data for autumn are incomplete (no data is available for the months of August and September), we expect a midday peak in the UFP concentration as observed in the Aitken mode particles – in August (Fig. S12). Given the nature of the location in Payerne (see Fig. S1), we expect the harvesting season to affect the concentration not only of the coarse particles but also of the ultrafine ones. In addition, earlier studies have shown a second wave of NPF events occurring during autumn when temperatures decrease allowing for better

350   condensation of gases into the particle phase (Dada et al., 2017). In the next sections we quantify the contribution of the primary and secondary sources to the total UFP concentrations.
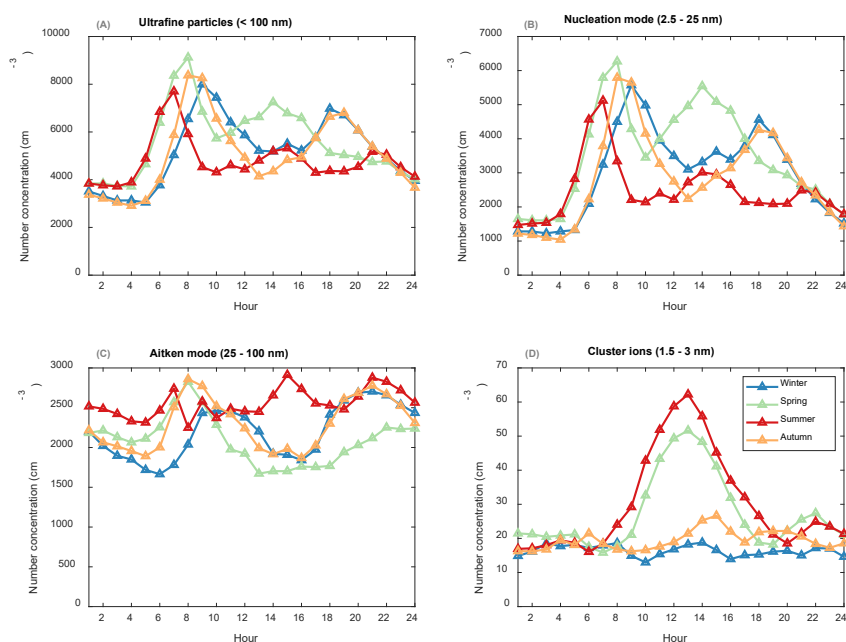
Figure 2 Seasonal diurnal average concentrations of (A) ultrafine, (B) nucleation mode and (C) Aitken mode particles and (D) cluster ions (positive) in Payerne. No data from August and September is available for the ultrafine and

355   nucleation mode particles or cluster ions. For the Aitken mode particles, July includes 2020 and 2021 concentrations. Data included in ultrafine, nucleation mode and cluster ion mode concentrations are in 5 min time steps (NAIS time stamp), while the Aitken mode concentrations are in 3 min time steps (SMPS time stamp). See monthly diurnal variations in Fig. S11.

4.3   Primary UFP at Payerne

360   #### 4.3.1   Non-volatile particles

The exact differentiation between primary and secondary particles is difficult at a receptor site because it depends on a lot of factors such as residence time, precursors etc. Nevertheless, the size-segregated number concentration measurement with the catalytic stripper allows for a rough estimation of primary particles, since these non-volatile particles are expected to consist mainly of refractory black carbon from incomplete combustion processes (Wang

365   et al., 2018), mostly from traffic and wood burning emissions. The secondary particles are in this study approximated as the difference between total and non-volatile particles. However, this approximation results in an overestimation of the secondary particles, since not all volatile particles necessarily are secondary in nature as for example traffic also emits primary volatile and semi-volatile UFPs (Baltensperger et al., 2002; Saarikoski et al., 2023). In Fig. 3, we show the particle number size distribution data retrieved from the total measurement, the

370   non-volatile measurement, and their difference (secondary particles) for an example day with a strong NPF event (17.02.2021). Based on our observation, the morning and evening traffic rush hours considerably increase the concentration of non-volatile particles consistent with our expectations that traffic emits black carbon particles.

Photo-chemically driven NPF starting before noon cause a distinct increase of total UFP concentration (Fig. 3A), which is entirely dominated by volatile particles as expected (see difference plot in Fig. 3C). The size distributions

375   of the non-volatile and secondary particles show distinct behavior in which the secondary particles contribute to smaller particles' concentration in the nucleation mode and reach higher diameters because of condensational growth. Secondary processes involving condensation facilitate the growth of particles until they reach climate relevant sizes, where they can contribute to regional scale phenomena e.g., regional NPF and cloud condensation nuclei (Zhou et al., 2021; Dai et al., 2017).
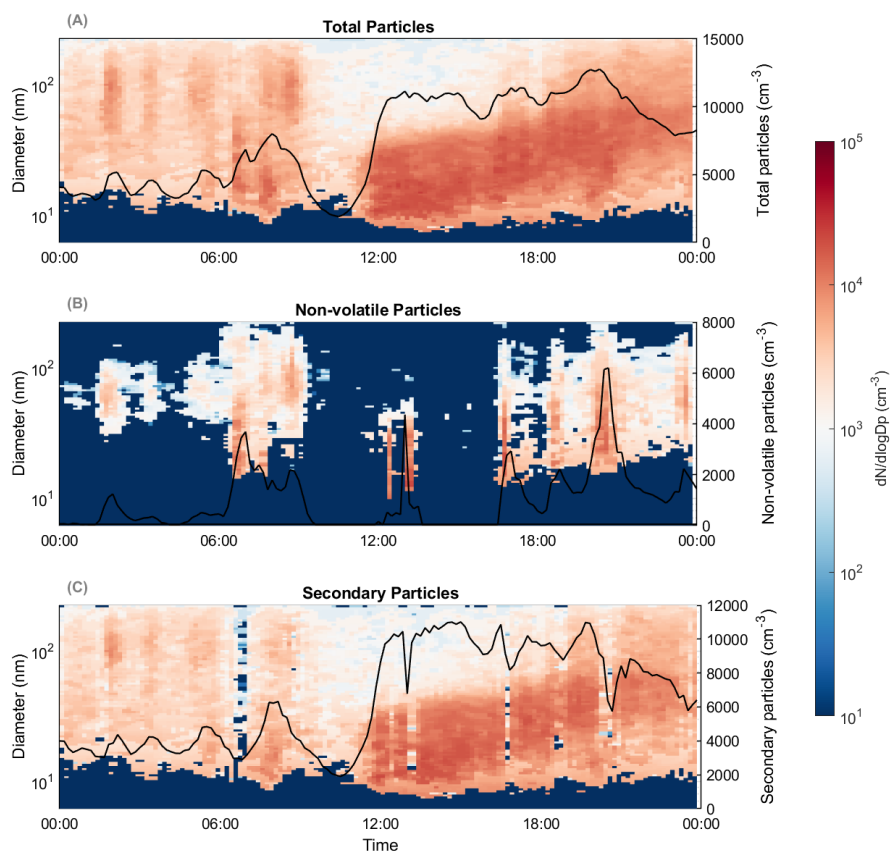
380

Figure 3 Particle number size distribution from (A) the total measurement, (B) the non-volatile measurement and (C) their difference (secondary particles) during a strong NPF event on 17.02.2021. The black solid lines relevant for the right axis show integrated number concentrations.

Using the ~3 months of available measurements (19.12.2020 – 3.3.2021), we quantified the contribution of

385 primary particles to the total UFPs and to each of the modes (Fig. 4, S13). We find a dominance of the secondary

particles on most days, except for few cases (discussed in detail in section 4.3.3). However, this method is subject

to limitations including:

1) Uncertainty on primary particles' number: quantifying primary particles through non-volatile particle

measurements produces a systematic low bias in estimated primary particle number as primary volatile

390 particles are misclassified as secondary particles.

2) Uncertainty on the size-distribution: Denuding volatile particulate matter from internally mixed particles

with a non-volatile core reduces their diameter. This affects the size distribution of secondary particle

calculated as the difference from total and non-volatile particle size distributions. Specifically, small

secondary particles may be underestimated, whereas larger secondary particles may be overestimated if a

395 substantial fraction of internally mixed primary non-volatile particles with a secondary coating is present.

3) Measurements only during a short period in winter might not be representative of the full year.

Given the limitations of this method, in the next section we compare it to a previously established method which uses BC as a tracer for primary particles.

4.3.2 BC tracer method

400 In this section, we used BC concentration as a tracer for estimating the number fraction of primary particles (Section 3.2). We first compare this method to the non-volatile measurements (section 4.3.1), and then to extend the analyses of primary and secondary particles to the full-year measurement period. For optimizing the BC-tracer method for Payerne, we assessed the sensitivity of choosing different percentiles (e.g. 0.1%, 0.5%, 1% and 2%) of observed N-to-BC ratios to infer the S_I factor in Eq. 2. The value of S_I showed low sensitivity to percentile

405 changes, as observed in previous locations (Rodríguez and Cuevas, 2007). Since, S_I is a simple factor used to estimate the number of primary particles per nanogram of BC, the low sensitivity of S_I to different percentiles directly translates to high precision of the estimated primary particle fraction (Fig. S14B). This approach does not systematically misclassify the primary volatile particles as secondary particles, whereas it has its own limitations. The approach is biased towards primary particle sources with the lowest N_{UFP}-to-BC ratio which in our case are

410 traffic-related particles (Rodríguez and Cuevas, 2007). A recent study estimated that the method leads to an overestimation of the primary vehicle exhaust particles concentrations by 18% and 26% in urban and suburban sites, respectively, but no impact on secondary particles (Casquero-Vera et al., 2021). However, given the overwhelming contribution of traffic related particles to BC compared to wood burning (Grange et al., 2020), and the association of the lowest N_{UFP}-to-BC to rush hours, and to wind direction opposite to the highway, we do not

415 expect large uncertainties in our estimation of the primary particle contribution.

In a next step, we compared the results from both methods (Fig. 4). Both methods agree best when the 1st percentile of the N_{UFP}-to-BC ratios is chosen as S_I. The results shown in Fig. 4 demonstrate the consistency between the results for the common measurement period, in winter, for all three size segregated fractions. As per the aforementioned limitations of both methods, both approaches likely represent a low estimate of the primary

420 particle fraction with the low biases expected to dominate over the high biases.

Our results, from both methods combined, suggest that, on average, 25% of the UFP in winter in Payerne originate from primary processes, while the remaining are formed in the atmosphere following oxidation of precursor gases or chemical processing of available aerosol particles. Based on the BC tracer method, 2.15 (x 10^6) cm^{-3} primary particles are observed per 1 ng/m^3 of BC. Our results are in line (slightly lower given the nature of our

425 measurement location) with previous measurements in Switzerland with 3.1 x 10^6 and 3.6 x 10^6 cm^{-3} primary particles per 1 ng/m^3 of BC observed in an urban background location in Lugano and an urban location in Bern, respectively (Reche et al., 2011), although differences in vehicle fleet between locations and changes over time due to more stringent emission regulations, are expected to influence this ratio. In comparison, less primary particles per 1 ng/m^3 BC are found in Payerne compared to other European cities such as Milan, Barcelona and

430 Santa Cruz de Tenerife, with values exceeding 4.5 (x 10^6) cm^{-3} primary particles per 1 ng/m^3 of BC (Rodríguez and Cuevas, 2007). In the next section, we extend the analyses over the full year of measurements using the BC tracer method.
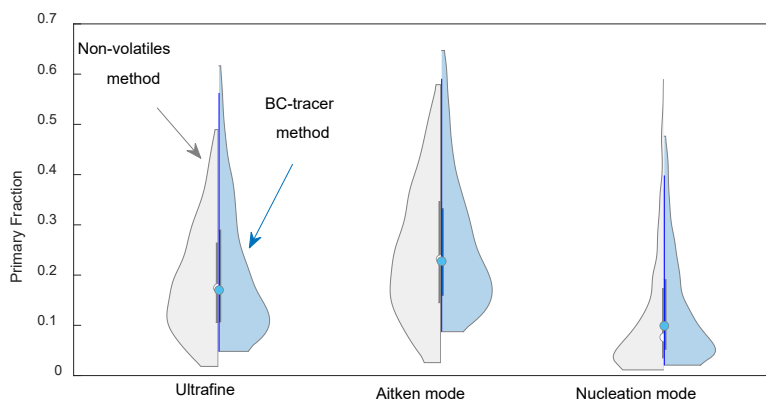
Figure 4 Fraction of primary particles in the ultrafine, Aitken and nucleation modes using the non-volatile particle measurements in gray and using the BC tracer method in blue. Violin plots are a combination of boxplot and a kernel distribution function on each side of the boxplots. The white circles define the median of the distribution and the edges on the inner grey boxes refer to the 25th and 75th percentiles, respectively. Plots include winter hourly averages, outliers below the 5th percentile or above the 95th percentile are excluded.

4.3.3 Seasonality of size-segregated primary and secondary UFPs

The longer-term results are not different from the wintertime observations: secondary particles dominate over primary ones (Fig. 5). In addition, during all seasons and for all size fractions, the higher particle concentration is associated with a higher secondary particle concentration, demonstrating the contribution of secondary processes to increasing the number of particles in the atmosphere (Fig. S15). The primary UFPs peak in the morning and evening is concurrent with traffic rush hours, while the secondary particles show morning and evening peaks and additionally a midday peak during the spring and summer seasons (Fig. 5D). While the diurnal variability of primary UFPs is controlled by both the nucleation and Aitken mode particles, the seasonal and diurnal variability of secondary UFPs is driven by the nucleation mode particles, which show a much higher contribution and variability.

We find that the nucleation mode is dominated by secondary particles with an average fraction of 84% contribution to the nucleation mode and 47% contribution to the total UFP (Fig. 5B-C). The primary nucleation mode particles are about two times higher in concentration in spring and summer compared to the colder seasons, with two peaks related to traffic rush hours as observed for the UFPs (Rönkkö et al., 2017). In comparison, the secondary fraction shows distinct seasonal patterns with a peak during midday only during warm seasons. Midday peaks are attributed to NPF events which are most intense during daytime – peak solar radiation (more details in section 4.4). Besides the NPF related peak during midday in warm seasons, the nucleation mode also exhibits a morning (all seasons) and evening peak (fall and winter season). The evening peak could be caused by biomass burning especially in winter (Casquero-Vera et al., 2021; Grange et al., 2020). The morning maximum of nucleation mode secondary particles occurs 1 to 2 hours after the peak of non-volatile primary traffic particles (Fig. 5F). Volatility and size suggest a secondary processing. The time lag indicates that it is not dominated by nucleation happening immediately after emission as the hot exhaust cools. Instead, it requires the accumulation of emitted vapors and/or chemical processing of these vapors.

In the Aitken mode, compared to the nucleation mode, we observe a higher contribution of primary particles, although the average fraction does not exceed 25% (Fig. 5C). In addition, while the primary Aitken mode particles display rush hour peaks, the secondary particles show a rather constant diurnal cycle (Fig. 5E). Primary Aitken mode particles originate from anthropogenic sources, i.e., traffic and residential wood burning. The secondary fraction is expected to comprise processed secondary particles emitted within a much larger spatial area (Seinfeld and Pandis, 2012).
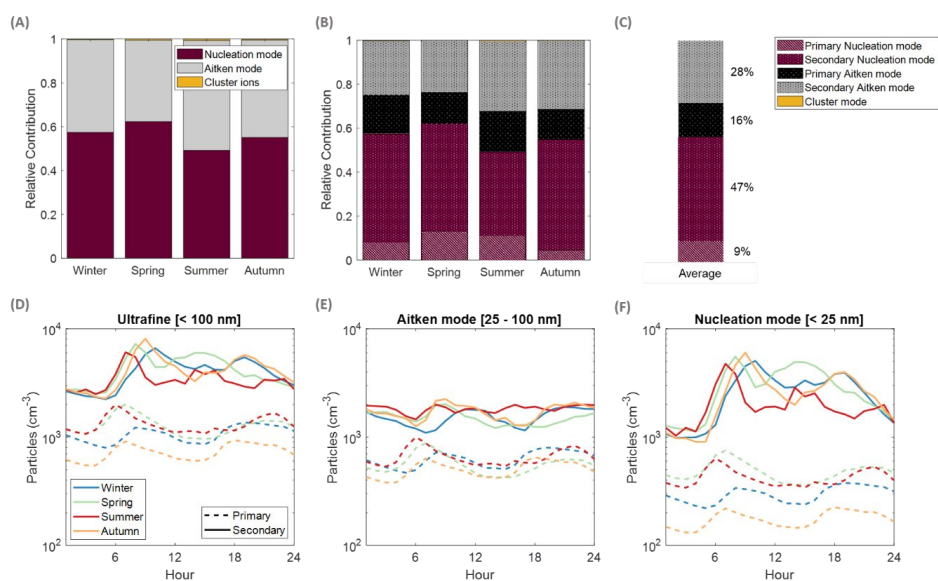
Figure 5 (A) Relative contribution of each of the nucleation and Aitken mode particles and cluster ions to total ultrafine particle concentrations. No data from August and September are available for the nucleation mode particles or cluster ions, affecting summer and autumn means. For the Aitken mode particles, summer July includes 2020 and 2021 concentrations. Data included in nucleation mode and cluster ion mode concentrations are in 5 min time steps (NAIS time stamp), while the Aitken mode concentrations are in 3 min time steps (SMPS time stamp). (B) Similar to (A) but with the inclusion of primary and secondary fractions. (C) Similar to (B) for the yearly average. For A, B and C, the color refers to the size fraction, while the shading pattern refers to the primary and secondary fractions. (D) The particle number concentration of the primary (dashed lines) and secondary (solid lines) in the ultrafine, (E) Aitken and (F) nucleation modes diurnal averages.

4.3.4   Sources of primary particles in Payerne

The BC-rich particles observed at Payerne can be attributed to wood burning and fossil fuel combustion emissions and are found in the fine mode having diameters smaller than 300 nm (Motos et al., 2020; Zotter et al., 2017; Grange et al., 2020). BC concentrations in Payerne are higher during winter compared to summer (Fig. S16 – S17), attributed to the higher contribution of wood burning for heating purposes together with a shallower boundary layer (Fig. S9). Traffic is another source of BC, which is depicted in our data as two daily peaks during rush hours: morning and evening (Fig. S16). Due to the proximity of our measurement site to the airport, BC-rich particles might be attributed to airport emissions. In Fig. S17, we assess potential influence of airport activities on the measured BC concentrations. Like SO_2, as discussed in section 4.1.2, the airport contribution to BC cannot be quantified, given the complexity of the sources around the measurement site. For instance, although the BC concentration drops by a factor of 1.3 during daytime weekends, this decrease could be attributed to a lower traffic

density. Additionally, BC concentrations do not decrease substantially during airport shutdown periods (Fig. S17). However, wind arriving from the airport direction (NW: 300 – 340˚) does not show elevated BC concentrations. These observations point toward a rather low influence of the airport to our BC measurements. Our findings fall in line with Grange et al. (2020) who attributed BC concentrations observed in Payerne, over the last decade, to residential wood burning and traffic emissions.

4.4 Secondary UFP at Payerne: the role of new particle formation events

4.4.1 Frequency of NPF events

A total of 266 days were classified into the event classes (defined in Sect. 3.2) as shown in Fig. S18. Among those, 154 days were classified as nonevent constituting 57% of the total days. 54 days (20%) were classified as local NPF event days, where the particle formation is observed starting from the smallest particles (sub-3 nm cluster ions) representing local processes. On 18 days (7%), an increase in ions concentration was observed with no increase in the larger particles or obvious signs of growth, these days were referred to as ion bumps. Both local NPF and ion bump events tended to occur more frequently during the warmer months, with local NPF events even occurring on most days (~70%) in May, while nonevent days occurred more frequently during the colder months (Fig. S19). The remainder of the days which did not fit the categories of either nonevent, local NPF, or ion bump were left undefined as these were either affected by precipitation or nearby traffic – elevated NO_2 concentrations. We note that we did not observe any transported events at the site, without a local NPF event.

4.4.2 Size-segregated growth rates

The particles formed in Payerne could grow to sizes greater than a few nm in most cases (local events). The median growth rates were 1.3, 3.4 and 5.0 nm.h^{-1} for the size ranges 1.5 – 3, 3 – 7 and 7 – 15 nm, respectively (Fig. S18). The GRs were comparable during the seasons within the same size fraction (Fig. S20). However, although slightly higher GRs are observed in summer compared to spring, this conclusion is not certain given the low statistics (Fig. S20). Still, higher growth rates are to be expected in warmer seasons given the increased emissions of biogenic VOCs (in case the condensation sink values are similar), especially in areas surrounded by vegetation as in Payerne.

Our measured GRs in the smallest size fractions (1.5 – 3 and 3 – 7 nm) are within the range of those observed in other rural environments, such as in Puy De Dome, France, (Manninen et al., 2010),Vavihill, Sweden, (Manninen et al., 2010), and the boreal forest in Hyytiälä, Finland, (Yli-Juuti et al., 2011). However, the GRs of the larger sizes exceed those observed in rural background locations and resemble more rural polluted locations such as Melpitz, Germany, and K-Puszta, Hungary, (Manninen et al., 2010). This observation might be attributed to the participation of anthropogenic sources (airport, heating and highway close to Payerne) to the growth (Fig. S1) together with lower CS (median CS$_{events}$ = 2.6 s^{-1}, see Fig. 6), compared to the rural polluted locations mentioned (median CS$_{events}$ (K-Puszta) = 6.6 s^{-1} and CS$_{events}$ (Melpitz) = 8.4 s^{-1})(Manninen et al., 2010).

4.4.3 Precursor vapors driving NPF at Payerne

A clear enhancement in the particle formation rate (total and ion induced) is observed on NPF event days compared to nonevent days. The median $J_{2.5}$ on event days is on average 2 times higher and during the peak up to

525   7 times higher than $J_{2.5}$ on nonevent days (Fig. 6A). The highest $J_{2.5}$ are observed during spring, with the highest
peak occurring in March and reaching up to 3 cm^{-3}s^{-1} (Fig. S21). These particle formation rates fall in the same
range as other rural and rather vegetation-dominated locations such as in Hyytiälä, Finland, (Kulmala et al., 2013),
Jarvseljä, Estonia, (Vana et al., 2016) and Hohenpeissenberg, Germany, (Birmili et al., 2003). The ion induced
formation rates ($J_{1.5}^-$ and $J_{1.5}^+$) show a similar trend as $J_{2.5}$ peaking around noon (Fig. 6B), especially in spring
530   (Fig. S21). Similarly, $J_{1.5}^+$ is 3 times and $J_{1.5}^-$ is 5 times on average higher on event days than on nonevent days.
During peak time, $J_{1.5}^+$ is 6 times and $J_{1.5}^-$ is 12 times higher on event days than on nonevent days. The factor of
2 difference between $J_{1.5}^+$ and $J_{1.5}^-$ could be attributed to the composition of air (Mohnen, 1976). As for $J_{2.5}$, average
$J_{1.5}^+$ and $J_{1.5}^-$ fall in the range of ion induced formation rates measured in rural locations in Europe, see Manninen
et al. (2010) and references therein.

535   At most locations in the continental boundary layer, sulfuric acid (H_2SO_4) mediates NPF events, especially in the
presence of fixing bases such as amines or ammonia (Yao et al., 2018; Dada et al., 2023; Almeida et al., 2013;
Kürten et al., 2016; Aktypis et al., 2024). At Payerne, NPF events are observed on days with enhanced of H_2SO_4
concentrations (calculated as a proxy from SO_2, see Sect. 3.4 - median events = 1.88 x 10^6 cm^{-3}, median nonevents
1.07 x 10^6 cm^{-3}) while SO_2 levels are similar on event and nonevent days (Fig. 6C, Fig. S22). Interestingly,
540   ammonia does not show a similar behavior, but an equal median concentration and distribution regardless of
whether an NPF event was observed or not (Fig. 6D). This observation allows us to conclude that while H_2SO_4
could be the factor controlling NPF in Payerne, ammonia is not the limiting factor. On the other hand, a clear
difference between CS levels is observed on events and nonevent days, so is the case for the cloudiness (median
CS_{events} = 2.7 x 10^{-3} s^{-1}, B_{events} = 0.72; median $CS_{nonevents}$ = 5.9 x 10^{-3} s^{-1}, $B_{nonevents}$ = 0.56) (Fig. 6E-F). The two
545   aforementioned factors control H_2SO_4 formation and hence an increased CS or cloudy conditions inhibit the
occurrence of NPF events. Based on these results, we can hypothesize that the limited H_2SO_4 formation (due to
high CS or cloudiness) could be the limiting factor for NPF in Payerne.
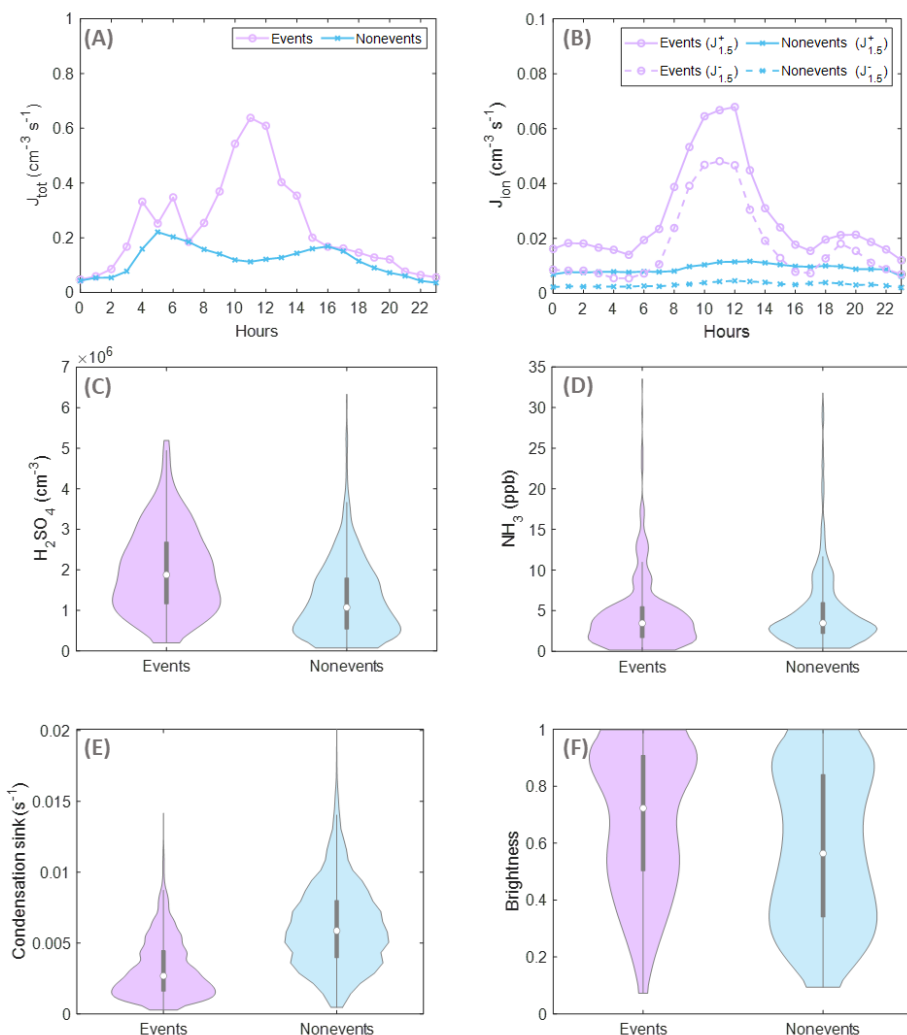
Figure 6 (A) total ($J_{2.5}$) and (B) ion induced ($J_{1.5}$) formation rates on event (pink) and nonevent days (blue). (C) H_2SO_4
550 **proxy concentration, (D) NH_3 concentration, (E) condensation sink and (F) brightness (clear-sky parameter) on event (pink) and nonevent days (blue) shown as violin plots. Violin plots are a combination of boxplot and a kernel distribution function on each side of the boxplots. The white circles define the median of the distribution and the edges on the inner grey boxes refer to the 25th and 75th percentiles, respectively.**

To confirm our hypothesis, we plot the observed NPF probability as a function of H_2SO_4 and CS in Fig. 7. We
555 find that events occurred most frequently under high H_2SO_4 exceeding 4×10^5 cm^{-3} and CS below 0.01 s^{-1} (Fig. 7). The highest probability is observed in the lower-right corner of Fig. 7, under high H_2SO_4 concentration and the lowest CS. As brightness and H_2SO_4 have a causal relationship, summer conditions favor H_2SO_4 formation, see also Fig. S23. SO_2 which is always available in the regional background air, has similar concentrations on event and nonevent days (Fig. S22), and higher concentrations are associated with air masses arriving from the northeast,
560 passing over the town of Payerne (Fig. S24). During less cloudy conditions (high B), SO_2 oxidation is favored, producing higher concentrations of H_2SO_4. At the same time, cleaner conditions (low CS), favor NPF occurrence

in two ways. First, the loss of H_2SO_4 to preexisting particles is decreased, favoring an increased lifetime of the precursor gas needed for NPF (see equation 6). Second, besides H_2SO_4, less freshly formed particles and precursor vapors needed for particle growth are lost, increasing the probability of NPF.
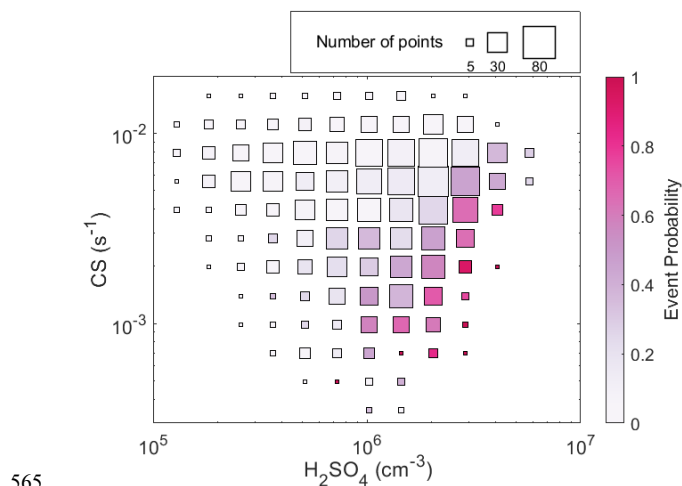
565

Figure 7 Event probability distribution at Payerne based on the CS and sulfuric acid proxy hourly concentrations during daytime [8:00 – 17:00 CET]. Marker size indicates number of days included in the probability calculation within every cell.

In Payerne, NPF events occurred most frequently when the wind arrived from the southwest areas dominated by
570   vegetation (grasslands and croplands) and associated with a lower CS suitable for NPF events to occur (Fig. S24-S25). Besides H_2SO_4, stabilizing bases are needed for NPF to occur in boundary layer conditions. In Switzerland, NH_3 and amines originate from agricultural practices, specifically from animal housing and manure storage and spreading especially in the central and western parts (Reidy et al., 2008). Wind carried similar NH_3 concentrations from all directions at our measurement site, as expected given the area's proximity to agricultural areas and
575   croplands (Fig. S24). As mentioned earlier, the NH_3 concentrations are also similar on NPF events and nonevent days, they are also sufficiently high to not limit NPF on days when sufficient H_2SO_4 is available. Although we have no amine measurements available, the wind direction carrying NH_3 is likely carrying amines as well. Amines such as methylamine, dimethylamine (DMA), and trimethylamine are expected to be abundant in rural locations in the vicinity of agricultural activities (Kürten et al., 2016; Ge et al., 2011).

580   By comparing our observations to previous field measurements and chamber experiments, we find that the data points from Payerne fall in the middle between all other measurement sites, boreal, rural and agricultural showing the complexity of the different sources (Fig. 8). During warmer periods, our data points fall in line with the measurements from the Po Valley, during spring. The authors of the Po Valley study report H_2SO_4-DMA as the main mechanism of NPF in this location aided by other bases such as NH_3; and estimate the NH_3 and DMA
585   concentrations to be 10.6 ppb and less than 10 ppt, respectively (Cai et al., 2024). Moreover, our data points fall at a slightly higher slope than those measured in an agricultural land in Finland (Qvidja – yellow circles [temperature from 5 to 25℃]) which were found to be mediated by H_2SO_4-NH_3 and extremely low volatility organic vapors of biogenic origin (Dada et al., 2023; Olin et al., 2022). Our data points fall on the same line as

H$_2$SO$_4$-DMA line (4 ppt DMA), based on kinetic-model parametrization at 25℃ from chamber experiments and
590   are higher than those parametrized from H$_2$SO$_4$-NH$_3$ experiments (Xiao et al., 2021). The scatter of the points and
deviation from the exact line can be largely attributed to the variable concentration of DMA as well as the
contribution of other vapors in the nucleation and growth process, e.g. biogenic and anthropogenic organics which
cannot be excluded.

Under colder temperature conditions, data points in Payerne coincide with measurements from Hyytiälä, where
595   the average H$_2$SO$_4$ concentrations are rather low, accompanied by a low average ammonia and DMA
concentrations, of 0.066 ppb and below detection limit, respectively (Hemmilä et al., 2018). However, the CS
levels are also comparably low (CS$_{events}$ = 1.4 x 10^{-3} s^{-1}), together with colder temperatures, favor NPF events at
these low concentrations. Hyytiälä forest site is also surrounded by a trees belt emitting monoterpenes, further
supporting particle nucleation and growth (Rinne et al., 2005). Similar to during warmer temperatures, the points
600   from Payerne fall on the same line as H$_2$SO$_4$-DMA line (4 pptv DMA), based on kinetic-model parametrization
at 5 ℃ from chamber experiments and at a higher slope than H$_2$SO$_4$-NH$_3$ chamber experiments (Xiao et al., 2021;
Lehtipalo et al., 2018).

Based on these observations, we can conclude that NPF events in Payerne are mediated by H$_2$SO$_4$-DMA supported
by ammonia, with the availability of H$_2$SO$_4$ (and low CS) being the decisive factor. Given the environment
605   surrounding our measurement location, we can speculate that both biogenic and anthropogenic organic vapors
contribute to the growth of the freshly formed particles. However, such conclusions can be only fully verified
with additional measurements of precursor vapors.
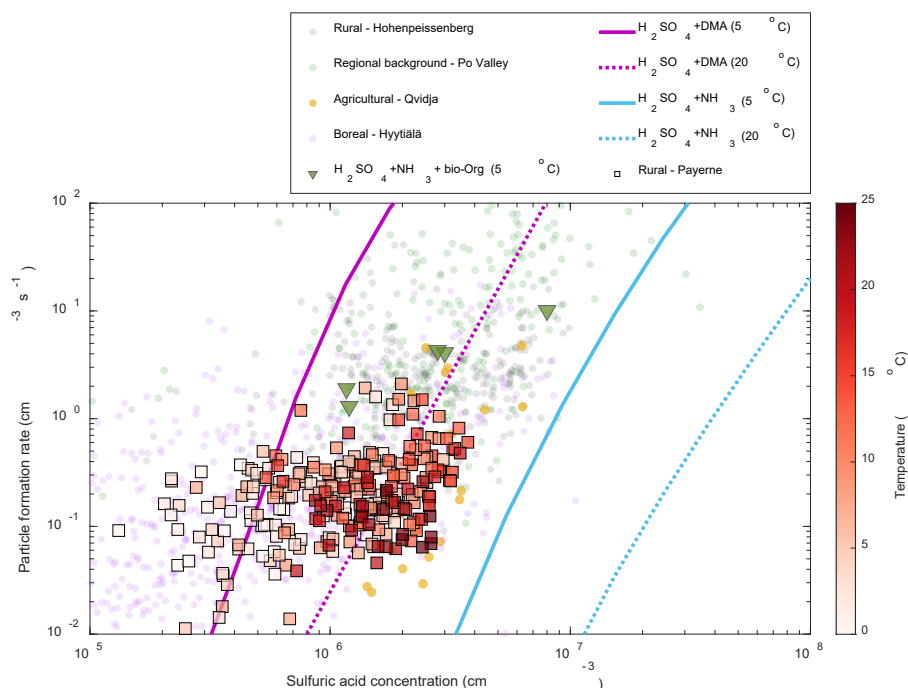
Figure 8 Particle formation rates as a function of H₂SO₄ concentration, daily averages (8:00 – 17:00 CET) – squares, are colored with ambient temperature. Parametrizations based on chamber measurements of H₂SO₄+NH₃ (2 ppbv) ammonia at 5°C (solid cyan line) and 20°C (dotted cyan line) are shown (Xiao et al., 2021). Similarly, parametrizations based on chamber measurements of H₂SO₄ + dimethylamine (DMA – 4pptv) at 5°C (solid magenta line) and 20°C (dotted magenta line) are shown (Xiao et al., 2021). Green triangles are H₂SO₄+NH₃ (0.1 – 1 ppbv) at 5°C in the presence of constant monoterpenes (α-pinene and Δ-3-carene) and NOx from Lehtipalo et al. (2018). Filled translucent points in the background are atmospheric measurement from the boreal forest (pink), rural location in Germany (grey)(Birmili et al., 2003), a regional background in Italy (green) (Cai et al., 2024) and an agricultural land (yellow)(Dada et al., 2023). Particle formation rates from chamber measurements are at 1.7 nm while field observations are either measured at 1.5 nm or extrapolated to 1.5 nm using the Kerminen and Kulmala equation (Kerminen and Kulmala, 2002) (see section 3.7). For Payerne, H₂SO₄ concentrations are derived from proxy calculations (see section 3.8).

4.4.4 Contribution of NPF particles to UFP

The analyses performed within the German Ultrafine Aerosol Network (GUAN) show that the contribution of NPF to UFPs was about 13 %, 21 %, and 7 % for the urban background, regional background, and low mountain range, respectively (Sun et al., 2024). We applied similar analyses to our data; although, our results might be subject to uncertainty due to low statistics especially during low radiation autumn or winter (Fig. S26). We found that the overall NPF contribution to the UFP was 5.07%. However, if we limit our analysis to the NPF time window (11:00 to 18:00 CEST), we find that the contribution of NPF to total UFP increased to 13.04%. Limiting our analysis further to the 3-hour peak NPF window, the contribution of NPF to total UFP increased to 20.4%. By combining the information on the secondary UFP fraction (section 4.3.3) with this analysis, we find that NPF explains an average of 6.8 % of the secondary UFP. A main reason for this low fraction is that the secondary particles also contain a substantial portion of volatile particles peaking shortly after the traffic rush hour, which are not counted in the NPF contribution.

We also performed the same analysis on the size segregated particles and found an overall contribution of NPF to nucleation mode particles of 9.32%, up to 21.3% during the NPF time window (11:00 to 18:00 CEST) and 32.1% during the 3-hour NPF peak. These results translate to ~20% contribution of NPF to secondary nucleation mode particles. On the other hand, the overall contribution of NPF to Aitken mode particles is near 0, even during the NPF time window. Such an observation is expected, as the Aitken mode particles are rather transported particles and not formed via local processes, see also section 4.3.3.

5 Conclusions

Understanding the sources of UFP in rural environments is crucial for assessing air quality, public health impacts, and the influence of both natural and anthropogenic emissions on regional atmospheric chemistry. In this work, we investigate the outdoor sources of UFPs at Payerne, an ACTRIS and NABEL site in rural Switzerland. Although UFPs in rural areas have not been as extensively studied as those in urban settings, our research demonstrates that secondary processes can elevate UFP concentrations in rural environments to levels similar to those found in urban areas. First, we identify and quantify primary and secondary UFP sources using long-term particle and ion number size distribution measurements starting from ~1 nm. By combining measurements of non-volatile particles and long-term BC concentrations, used as tracers for primary particles, we find that secondary particles dominate the overall particle size distribution, with a larger fraction at higher particle concentrations demonstrating the role of atmospheric processing in increasing the number concentration of particles in the atmosphere.

Primary particles in Payerne comprise those originating from traffic and wood burning. While the concentrations are relatively similar between the different seasons, the diurnal pattern shows the unique peaks concurrent with morning and evening traffic rush hours. In comparison, secondary particles, originate from NPF events and processing of primary particles. UFPs diurnal and seasonal variability is determined by the nucleation mode particles dominating in spring and summer due to local emissions and secondary aerosol formation. NPF happens in spring and summer and contributes largely to the nucleation mode (~ 20%). Based on several lines of evidence, we find that NPF events in Payerne are driven by H_2SO_4 and stabilizing bases likely DMA supported by ammonia, with the availability of H_2SO_4 in combination with sufficiently low CS being the decisive factor. Given the location and multitude of sources, it is likely that both biogenic and anthropogenic organic vapors contribute to the growth of the newly formed particles. However, additional measurements of precursor vapors are needed to fully verify these conclusions.

6 Acknowledgements

We acknowledge Maxime Hervo, Alexander Häfele and Phillippe Overney from MeteoSwiss in Payerne for providing the infrastructure access and support with the measurements. We further acknowledge MeteoSwiss collaborators at Payerne for the operational SMN and EMER-Met measurements. Nicolas Bukowiecki is further acknowledged for his contribution to the fund raising of the GAW-CH science project that initiated the aerosol insitu measurements in Payerne. Günther Wehrle, Pascal Schneider and Levi Folghera are acknowledged for the

technical support of the aerosol in situ observations. We also thank Kaspar R. Daellenbach for scientific discussions.

670 **7   Funding**

Initial pilot implementation of aerosol in situ measurements at the Payerne observatory received financial support from MeteoSwiss through a science project in the framework of the Swiss contribution to the Global Atmosphere Watch programme (GAW-CH) of the World Meteorological Organization. Further upgrades and operation of the ACTRIS observations at Payerne were funded by the Swiss State Secretariat for Education and Research and

675 Innovation (SERI) in the framework of ACTRIS Switzerland. Further operation support was received from topical centers of the ACTRIS ERIC. L.D. acknowledges funding from the SNSF (grant number 216181). N.E. thanks cross-atmospheric research infrastructure services provided by ATMO-ACCESS (EU grant agreement No 101008004).

8   Author Contributions

680 Conceptualization: LD

Fund raising: MGB, BB

Data collection: BB, MCC, CH, MS

Data Analysis: BB, NN, LA, LD, MCC, CH, MS

Data interpretation and scientific discussions: all

685 Writing: LD

Review and commenting: all

9   Conflict of interest

The authors declare no conflict of interest.

10   Data availability

690 Global radiation, temperature, precipitation, wind speed and wind direction data can be obtained from the SwissMetNet   (https://opendata.swiss/de/dataset/automatische-meteorologische-bodenmessstationen).   Trace gases data are available open access on the National Air Pollution Monitoring Network (NABEL) website (https://www.bafu.admin.ch/bafu/en/home/topics/air/state/data/data-query-nabel.html). All other data would be provided from the corresponding authors upon request.

695

11   References

Aktypis, A., Kaltsonoudis, C., Patoulias, D., Kalkavouras, P., Matrali, A., Vasilakopoulou, C. N., Kostenidou, E., Florou, K., Kalivitis, N., Bougiatioti, A., Eleftheriadis, K., Vratolis, S., Gini, M. I., Kouras, A., Samara, C., Lazaridis, M., Chatoutsidou, S. E., Mihalopoulos, N., and Pandis, S. N.: Significant spatial gradients in new particle formation frequency in Greece during summer, Atmos. Chem. Phys., 24, 65-84, 10.5194/acp-24-65-2024, 2024.

Almeida, J., Schobesberger, S., Kurten, A., Ortega, I. K., Kupiainen-Maatta, O., Praplan, A. P., Adamov, A., Amorim, A., Bianchi, F., Breitenlechner, M., David, A., Dommen, J., Donahue, N. M., Downard, A., Dunne, E., Duplissy, J., Ehrhart, S., Flagan, R. C., Franchin, A., Guida, R., Hakala, J., Hansel, A., Heinritzi, M., Henschel, H., Jokinen, T., Junninen, H., Kajos, M., Kangasluoma, J., Keskinen, H., Kupc, A., Kurten, T., Kvashin, A. N., Laaksonen, A., Lehtipalo, K., Leiminger, M., Leppa, J., Loukonen, V., Makhmutov, V., Mathot, S., McGrath, M. J., Nieminen, T., Olenius, T., Onnela, A., Petaja, T., Riccobono, F., Riipinen, I., Rissanen, M., Rondo, L., Ruuskanen, T., Santos, F. D., Sarnela, N., Schallhart, S., Schnitzhofer, R., Seinfeld, J. H., Simon, M., Sipila, M., Stozhkov, Y., Stratmann, F., Tome, A., Trostl, J., Tsagkogeorgas, G., Vaattovaara, P., Viisanen, Y., Virtanen, A., Vrtala, A., Wagner, P. E., Weingartner, E., Wex, H., Williamson, C., Wimmer, D., Ye, P. L., Yli-Juuti, T., Carslaw, K. S., Kulmala, M., Curtius, J., Baltensperger, U., Worsnop, D. R., Vehkamaki, H., and Kirkby, J.: Molecular understanding of sulphuric acid-amine particle nucleation in the atmosphere, Nature, 502, 359-363, 10.1038/nature12663, 2013.

Baltensperger, U., Streit, N., Weingartner, E., Nyeki, S., Prévôt, A. S. H., Van Dingenen, R., Virkkula, A., Putaud, J.-P., Even, A., ten Brink, H., Blatter, A., Neftel, A., and Gäggeler, H. W.: Urban and rural aerosol characterization of summer smog events during the PIPAPO field campaign in Milan, Italy, Journal of Geophysical Research: Atmospheres, 107, LOP 6-1-LOP 6-14, 10.1029/2001JD001292, 2002.

Bianchi, F., Tröstl, J., Junninen, H., Frege, C., Henne, S., Hoyle, C., Molteni, U., Herrmann, E., Adamov, A., Bukowiecki, N., Chen, X., Duplissy, J., Gysel, M., Hutterli, M., Kangasluoma, J., Kontkanen, J., Kürten, A., Manninen, H. E., Münch, S., Peräkylä, O., Petäjä, T., Rondo, L., Williamson, C., Weingartner, E., Curtius, J., Worsnop, D. R., Kulmala, M., Dommen, J., and Baltensperger, U.: New particle formation in the free troposphere: A question of chemistry and timing, Science, 352, 1109-1112, 10.1126/science.aad5456, 2016.

Birmili, W., Berresheim, H., Plass-Dulmer, C., Elste, T., Gilge, S., Wiedensohler, A., and Uhrner, U.: The Hohenpeissenberg aerosol formation experiment (HAFEX): a long-term study including size-resolved aerosol, H2SO4, OH, and monoterpenes measurements, Atmos Chem Phys, 3, 361-376, 10.5194/acp-3-361-2003, 2003.

Bukowiecki, N., Dommen, J., Prévôt, A. S. H., Richter, R., Weingartner, E., and Baltensperger, U.: A mobile pollutant measurement laboratory—measuring gas phase and aerosol ambient concentrations with high spatial and temporal resolution, Atmospheric Environment, 36, 5569-5579, 10.1016/S1352-2310(02)00694-5, 2002.

Cai, J., Sulo, J., Gu, Y., Holm, S., Cai, R., Thomas, S., Neuberger, A., Mattsson, F., Paglione, M., Decesari, S., Rinaldi, M., Yin, R., Aliaga, D., Huang, W., Li, Y., Gramlich, Y., Ciarelli, G., Quéléver, L., Sarnela, N., Lehtipalo, K., Zannoni, N., Wu, C., Nie, W., Kangasluoma, J., Mohr, C., Kulmala, M., Zha, Q., Stolzenburg, D., and Bianchi, F.: Elucidating the mechanisms of atmospheric new particle formation in the highly polluted Po Valley, Italy, Atmos. Chem. Phys., 24, 2423-2441, 10.5194/acp-24-2423-2024, 2024.

Cai, J., Chu, B. W., Yao, L., Yan, C., Heikkinen, L. M., Zheng, F. X., Li, C., Fan, X. L., Zhang, S. J., Yang, D. Y., Wang, Y. H., Kokkonen, T. V., Chan, T., Zhou, Y., Dada, L., Liu, Y. C., He, H., Paasonen, P., Kujansuu, J. T., Petäjä, T., Mohr, C., Kangasluoma, J., Bianchi, F., Sun, Y. L., Croteau, P. L., Worsnop, D. R., Kerminen, V. M., Du, W., Kulmala, M., and Daellenbach, K. R.: Size-segregated particle number and mass concentrations from different emission sources in urban Beijing, Atmos Chem Phys, 20, 12721-12740, 10.5194/acp-20-12721-2020, 2020.

Casquero-Vera, J. A., Lyamani, H., Titos, G., Minguillón, M. C., Dada, L., Alastuey, A., Querol, X., Petäjä, T., Olmo, F. J., and Alados-Arboledas, L.: Quantifying traffic, biomass burning and secondary source contributions to atmospheric particle number concentrations at urban and suburban sites, Science of The Total Environment, 768, 145282, 10.1016/j.scitotenv.2021.145282, 2021.

Chen, G., Canonaco, F., Tobler, A., Aas, W., Alastuey, A., Allan, J., Atabakhsh, S., Aurela, M., Baltensperger, U., Bougiatioti, A., De Brito, J. F., Ceburnis, D., Chazeau, B., Chebaicheb, H., Daellenbach, K. R., Ehn, M., El

Haddad, I., Eleftheriadis, K., Favez, O., Flentje, H., Font, A., Fossum, K., Freney, E., Gini, M., Green, D. C., Heikkinen, L., Herrmann, H., Kalogridis, A.-C., Keernik, H., Lhotka, R., Lin, C., Lunder, C., Maasikmets, M., Manousakas, M. I., Marchand, N., Marin, C., Marmureanu, L., Mihalopoulos, N., Močnik, G., Nęcki, J., O'Dowd, C., Ovadnevaite, J., Peter, T., Petit, J.-E., Pikridas, M., Matthew Platt, S., Pokorná, P., Poulain, L., Priestman, M.,
750 Riffault, V., Rinaldi, M., Różański, K., Schwarz, J., Sciare, J., Simon, L., Skiba, A., Slowik, J. G., Sosedova, Y., Stavroulas, I., Styszko, K., Teinemaa, E., Timonen, H., Tremper, A., Vasilescu, J., Via, M., Vodička, P., Wiedensohler, A., Zografou, O., Cruz Minguillón, M., and Prévôt, A. S. H.: European aerosol phenomenology − 8: Harmonised source apportionment of organic aerosol using 22 Year-long ACSM/AMS datasets, Environment International, 166, 107325, 10.1016/j.envint.2022.107325, 2022.

755 Collaud Coen, M., Praz, C., Haefele, A., Ruffieux, D., Kaufmann, P., and Calpini, B.: Determination and climatology of the planetary boundary layer height above the Swiss plateau by in situ and remote sensing measurements as well as by the COSMO-2 model, Atmos. Chem. Phys., 14, 13205-13221, 10.5194/acp-14-13205-2014, 2014.

Dada, L., Chellapermal, R., Buenrostro Mazon, S., Paasonen, P., Lampilahti, J., Manninen, H. E., Junninen, H.,
760 Petäjä, T., Kerminen, V. M., and Kulmala, M.: Refined classification and characterization of atmospheric new-particle formation events using air ions, Atmos. Chem. Phys., 18, 17883-17893, 10.5194/acp-18-17883-2018, 2018.

Dada, L., Paasonen, P., Nieminen, T., Mazon, S. B., Kontkanen, J., Perakyla, O., Lehtipalo, K., Hussein, T., Petaja, T., Kerminen, V. M., Back, J., and Kulmala, M.: Long-term analysis of clear-sky new particle formation
765 events and nonevents in Hyytiala, Atmos Chem Phys, 17, 6227-6241, 10.5194/acp-17-6227-2017, 2017.

Dada, L., Lehtipalo, K., Kontkanen, J., Nieminen, T., Baalbaki, R., Ahonen, L., Duplissy, J., Yan, C., Chu, B., Petäjä, T., Lehtinen, K., Kerminen, V.-M., Kulmala, M., and Kangasluoma, J.: Formation and growth of sub-3-nm aerosol particles in experimental chambers, Nature Protocols, 15, 1013-1040, 10.1038/s41596-019-0274-z, 2020b.

770 Dada, L., Okuljar, M., Shen, J., Olin, M., Wu, Y., Heimsch, L., Herlin, I., Kankaanrinta, S., Lampimäki, M., Kalliokoski, J., Baalbaki, R., Lohila, A., Petäjä, T., Maso, M. D., Duplissy, J., Kerminen, V.-M., and Kulmala, M.: The synergistic role of sulfuric acid, ammonia and organics in particle formation over an agricultural land, Environmental Science: Atmospheres, 10.1039/D3EA00065F, 2023.

Dada, L., Ylivinkka, I., Baalbaki, R., Li, C., Guo, Y., Yan, C., Yao, L., Sarnela, N., Jokinen, T., Daellenbach, K.
775 R., Yin, R., Deng, C., Chu, B., Nieminen, T., Wang, Y., Lin, Z., Thakur, R. C., Kontkanen, J., Stolzenburg, D., Sipilä, M., Hussein, T., Paasonen, P., Bianchi, F., Salma, I., Weidinger, T., Pikridas, M., Sciare, J., Jiang, J., Liu, Y., Petäjä, T., Kerminen, V. M., and Kulmala, M.: Sources and sinks driving sulfuric acid concentrations in contrasting environments: implications on proxy calculations, Atmos. Chem. Phys., 20, 11747-11766, 10.5194/acp-20-11747-2020, 2020.

780 Dai, L., Wang, H., Zhou, L., An, J., Tang, L., Lu, C., Yan, W., Liu, R., Kong, S., Chen, M., Lee, S., and Yu, H.: Regional and local new particle formation events observed in the Yangtze River Delta region, China, Journal of Geophysical Research: Atmospheres, 122, 2389-2402, 10.1002/2016JD026030, 2017.

Dal Maso, M., Kulmala, M., Riipinen, I., Wagner, R., Hussein, T., Aalto, P. P., and Lehtinen, K. E. J.: Formation and growth of fresh atmospheric aerosols: eight years of aerosol size distribution data from SMEAR II, Hyytiala,
785 Finland, Boreal Environment Research, 10, 323-336, 2005.

Durdina, L., Brem, B. T., Setyan, A., Siegerist, F., Rindlisbacher, T., and Wang, J.: Assessment of Particle Pollution from Jetliners: from Smoke Visibility to Nanoparticle Counting, Environmental Science & Technology, 51, 3534-3541, 10.1021/acs.est.6b05801, 2017.

EEA: Switzerland – air pollution country fact sheet : https://www.eea.europa.eu/themes/air/country-fact-
790 sheets/2023-country-fact-sheets/switzerland-air-pollution-country, 2023.

Eeftens, M., Phuleria, H. C., Meier, R., Aguilera, I., Corradi, E., Davey, M., Ducret-Stich, R., Fierz, M., Gehrig, R., Ineichen, A., Keidel, D., Probst-Hensch, N., Ragettli, M. S., Schindler, C., Künzli, N., and Tsai, M.-Y.: Spatial and temporal variability of ultrafine particles, NO2, PM2.5, PM2.5 absorbance, PM10 and PMcoarse in Swiss study areas, Atmospheric Environment, 111, 60-70, 10.1016/j.atmosenv.2015.03.031, 2015.

795   EMEP/CCC: EMEP manual for sampling and chemical analysis: https://projects.nilu.no/ccc/manual/download/cccr1-95rev.pdf, 2001.

EMPA and BAFU: Technischer Bericht zum Nationalen Beobachtungsnetz für Luftfremdstoffe (NABEL) 2023: https://www.bafu.admin.ch/dam/bafu/de/dokumente/luft/fachinfo-daten/technischer_berichtzumnationalenbeobachtungsnetzfuerluftfremdsto.pdf.download.pdf/technischer_berich
800   tzumnationalenbeobachtungsnetzfuerluftfremdsto.pdf, 2023.

FOEN: Air Quality and Pollution Control in Switzerland: https://www.bafu.admin.ch, Swiss Federal Office for the Environment 2021.

Gagne, S., Lehtipalo, K., Manninen, H. E., Nieminen, T., Schobesberger, S., Franchin, A., Yli-Juuti, T., Boulon, J., Sonntag, A., Mirme, S., Mirme, A., Horrak, U., Petaja, T., Asmi, E., and Kulmala, M.: Intercomparison of air
805   ion spectrometers: an evaluation of results in varying conditions, Atmospheric Measurement Techniques, 4, 805-822, 10.5194/amt-4-805-2011, 2011.

Ge, X., Wexler, A. S., and Clegg, S. L.: Atmospheric amines – Part I. A review, Atmospheric Environment, 45, 524-546, 10.1016/j.atmosenv.2010.10.012, 2011.

Grange, S. K., Lötscher, H., Fischer, A., Emmenegger, L., and Hueglin, C.: Evaluation of equivalent black carbon
810   source apportionment using observations from Switzerland between 2008 and 2018, Atmos. Meas. Tech., 13, 1867-1885, 10.5194/amt-13-1867-2020, 2020.

Grange, S. K., Fischer, A., Zellweger, C., Alastuey, A., Querol, X., Jaffrezo, J.-L., Weber, S., Uzu, G., and Hueglin, C.: Switzerland's PM10 and PM2.5 environmental increments show the importance of non-exhaust emissions, Atmospheric Environment: X, 12, 100145, 10.1016/j.aeaoa.2021.100145, 2021.

815   Haeberle, L., Stoelzle, W., and Sievers, T. F.: Business Aviation Study Switzerland 2022: https://www.zhk.ch/fileadmin/user_upload/redakteure/PDF/Studien_Factsheets/Business_Aviation_Study_Switzerland_full_version.pdf, 2022.

Hemmilä, M., Hellén, H., Virkkula, A., Makkonen, U., Praplan, A. P., Kontkanen, J., Ahonen, L., Kulmala, M., and Hakola, H.: Amines in boreal forest air at SMEAR II station in Finland, Atmos. Chem. Phys., 18, 6367-6380,
820   10.5194/acp-18-6367-2018, 2018.

Jion, M. M. M. F., Jannat, J. N., Mia, M. Y., Ali, M. A., Islam, M. S., Ibrahim, S. M., Pal, S. C., Islam, A., Sarker, A., Malafaia, G., Bilal, M., and Islam, A. R. M. T.: A critical review and prospect of NO2 and SO2 pollution over Asia: Hotspots, trends, and sources, Science of The Total Environment, 876, 162851, https://doi.org/10.1016/j.scitotenv.2023.162851, 2023.

825   Kangasluoma, J., Cai, R., Jiang, J., Deng, C., Stolzenburg, D., Ahonen, L. R., Chan, T., Fu, Y., Kim, C., Laurila, T. M., Zhou, Y., Dada, L., Sulo, J., Flagan, R. C., Kulmala, M., Petäjä, T., and Lehtipalo, K.: Overview of measurements and current instrumentation for 1–10 nm aerosol particle number size distributions, Journal of Aerosol Science, 148, 105584, 10.1016/j.jaerosci.2020.105584, 2020.

Kerminen, V.-M. and Kulmala, M.: Analytical formulae connecting the "real" and the "apparent" nucleation rate
830   and the nuclei number concentration for atmospheric nucleation events, Journal of Aerosol Science, 33, 609-622, 10.1016/S0021-8502(01)00194-X, 2002.

Kerminen, V.-M., Chen, X., Vakkari, V., Petäjä, T., Kulmala, M., and Bianchi, F.: Atmospheric new particle formation and growth: review of field observations, Environ. Res. Lett., 13, 103003, 10.1088/1748-9326/aadf3c, 2018.

835   Kittelson, D. B., Watts, W. F., Johnson, J. P., Remerowki, M. L., Ische, E. E., Oberdörster, G., Gelein, R. M., Elder, A., Hopke, P. K., Kim, E., Zhao, W., Zhou, L., and Jeong, C. H.: On-Road Exposure to Highway Aerosols. 1. Aerosol and Gas Measurements, Inhalation Toxicology, 16, 31-39, 10.1080/08958370490443024, 2004.

Kulmala, M., Vehkamäki, H., Petäjä, T., Dal Maso, M., Lauri, A., Kerminen, V.-M., Birmili, W., and McMurry, P. H.: Formation and growth rates of ultrafine atmospheric particles: a review of observations, Journal of Aerosol
840   Science, 35, 143-176, 10.1016/j.jaerosci.2003.10.003, 2004.

Kulmala, M., Dal Maso, M., Makela, J. M., Pirjola, L., Vakeva, M., Aalto, P., Miikkulainen, P., Hameri, K., and O'Dowd, C. D.: On the formation, growth and composition of nucleation mode particles, Tellus Series B-Chemical and Physical Meteorology, 53, 479-490, 10.1034/j.1600-0889.2001.d01-33.x, 2001.

845   Kulmala, M., Luoma, K., Virkkula, A., Petaja, T., Paasonen, P., Kerminen, V. M., Nie, W., Qi, X. M., Shen, Y. C., Chi, X. G., and Ding, A. J.: On the mode-segregated aerosol particle number concentration load: contributions of primary and secondary particles in Hyytiala and Nanjing, Boreal Environment Research, 21, 319-331, 2016.

Kulmala, M., Petaja, T., Nieminen, T., Sipila, M., Manninen, H. E., Lehtipalo, K., Dal Maso, M., Aalto, P. P., Junninen, H., Paasonen, P., Riipinen, I., Lehtinen, K. E. J., Laaksonen, A., and Kerminen, V. M.: Measurement of the nucleation of atmospheric aerosol particles, Nature Protocols, 7, 1651-1667, 10.1038/nprot.2012.091, 2012.

850   Kulmala, M., Junninen, H., Dada, L., Salma, I., Weidinger, T., Thén, W., Vörösmarty, M., Komsaare, K., Stolzenburg, D., Cai, R., Yan, C., Li, X., Deng, C., Jiang, J., Petäjä, T., Nieminen, T., and Kerminen, V.-M.: Quiet New Particle Formation in the Atmosphere, Frontiers in Environmental Science, 10, 10.3389/fenvs.2022.912385, 2022.

Kulmala, M., Kontkanen, J., Junninen, H., Lehtipalo, K., Manninen, H. E., Nieminen, T., Petaja, T., Sipila, M.,
855   Schobesberger, S., Rantala, P., Franchin, A., Jokinen, T., Jarvinen, E., Aijala, M., Kangasluoma, J., Hakala, J., Aalto, P. P., Paasonen, P., Mikkila, J., Vanhanen, J., Aalto, J., Hakola, H., Makkonen, U., Ruuskanen, T., Mauldin, R. L., Duplissy, J., Vehkamaki, H., Back, J., Kortelainen, A., Riipinen, I., Kurten, T., Johnston, M. V., Smith, J. N., Ehn, M., Mentel, T. F., Lehtinen, K. E. J., Laaksonen, A., Kerminen, V. M., and Worsnop, D. R.: Direct Observations of Atmospheric Aerosol Nucleation, Science, 339, 943-946, 10.1126/science.1227385, 2013.

860   Kürten, A., Bergen, A., Heinritzi, M., Leiminger, M., Lorenz, V., Piel, F., Simon, M., Sitals, R., Wagner, A. C., and Curtius, J.: Observation of new particle formation and measurement of sulfuric acid, ammonia, amines and highly oxidized organic molecules at a rural site in central Germany, Atmos. Chem. Phys., 16, 12793-12813, 10.5194/acp-16-12793-2016, 2016.

Kwon, H.-S., Ryu, M. H., and Carlsten, C.: Ultrafine particles: unique physicochemical properties relevant to
865   health and disease, Experimental & Molecular Medicine, 52, 318-328, 10.1038/s12276-020-0405-1, 2020.

Lehtipalo, K., Yan, C., Dada, L., Bianchi, F., Xiao, M., Wagner, R., Stolzenburg, D., Ahonen, L. R., Amorim, A., Baccarini, A., Bauer, P. S., Baumgartner, B., Bergen, A., Bernhammer, A.-K., Breitenlechner, M., Brilke, S., Buchholz, A., Mazon, S. B., Chen, D., Chen, X., Dias, A., Dommen, J., Draper, D. C., Duplissy, J., Ehn, M., Finkenzeller, H., Fischer, L., Frege, C., Fuchs, C., Garmash, O., Gordon, H., Hakala, J., He, X., Heikkinen, L.,
870   Heinritzi, M., Helm, J. C., Hofbauer, V., Hoyle, C. R., Jokinen, T., Kangasluoma, J., Kerminen, V.-M., Kim, C., Kirkby, J., Kontkanen, J., Kürten, A., Lawler, M. J., Mai, H., Mathot, S., Mauldin, R. L., Molteni, U., Nichman, L., Nie, W., Nieminen, T., Ojdanic, A., Onnela, A., Passananti, M., Petäjä, T., Piel, F., Pospisilova, V., Quéléver, L. L. J., Rissanen, M. P., Rose, C., Sarnela, N., Schallhart, S., Schuchmann, S., Sengupta, K., Simon, M., Sipilä, M., Tauber, C., Tomé, A., Tröstl, J., Väisänen, O., Vogel, A. L., Volkamer, R., Wagner, A. C., Wang, M., Weitz,
875   L., Wimmer, D., Ye, P., Ylisirniö, A., Zha, Q., Carslaw, K. S., Curtius, J., Donahue, N. M., Flagan, R. C., Hansel, A., Riipinen, I., Virtanen, A., Winkler, P. M., Baltensperger, U., Kulmala, M., and Worsnop, D. R.: Multicomponent new particle formation from sulfuric acid, ammonia, and biogenic vapors, Science Advances, 4, eaau5363, 10.1126/sciadv.aau5363 2018.

Liscinsky, D. and Hollick, H.: Effect of particle sampling technique and transport on particle penetration at the
880   high temperature and pressure conditions found in gas turbine combustors and engines, NASA contractor report, NASA/CR-2010-NNC07CB03C, 2010.

Ma, N. and Birmili, W.: Estimating the contribution of photochemical particle formation to ultrafine particle number averages in an urban atmosphere, Science of The Total Environment, 512-513, 154-166, 10.1016/j.scitotenv.2015.01.009, 2015.

885   Manninen, H. E., Nieminen, T., Asmi, E., Gagne, S., Hakkinen, S., Lehtipalo, K., Aalto, P., Vana, M., Mirme, A., Mirme, S., Horrak, U., Plass-Dulmer, C., Stange, G., Kiss, G., Hoffer, A., Toeroe, N., Moerman, M., Henzing, B., de Leeuw, G., Brinkenberg, M., Kouvarakis, G. N., Bougiatioti, A., Mihalopoulos, N., O'Dowd, C., Ceburnis, D., Arneth, A., Svenningsson, B., Swietlicki, E., Tarozzi, L., Decesari, S., Facchini, M. C., Birmili, W., Sonntag, A., Wiedensohler, A., Boulon, J., Sellegri, K., Laj, P., Gysel, M., Bukowiecki, N., Weingartner, E., Wehrle, G.,
890   Laaksonen, A., Hamed, A., Joutsensaari, J., Petaja, T., Kerminen, V. M., and Kulmala, M.: EUCAARI ion

spectrometer measurements at 12 European sites - analysis of new particle formation events, Atmos Chem Phys, 10, 7907-7927, 10.5194/acp-10-7907-2010, 2010.

Maricq, M. M., Podsiadlik, D. H., Brehob, D. D., and Haghgooie, M.: Particulate Emissions from a Direct-Injection Spark-Ignition (DISI) Engine, 10.4271/1999-01-1530, 1999.

895   Meier, R., Eeftens, M., Aguilera, I., Phuleria, H. C., Ineichen, A., Davey, M., Ragettli, M. S., Fierz, M., Schindler, C., Probst-Hensch, N., Tsai, M.-Y., and Künzli, N.: Ambient Ultrafine Particle Levels at Residential and Reference Sites in Urban and Rural Switzerland, Environmental Science & Technology, 49, 2709-2715, 10.1021/es505246m, 2015.

Mohnen, V. A.: Formation, Nature, and Mobility of Ions of Atmospheric Importance, Dolezalek, H., Reiter, R.,
900   Landsberg, H.E. (eds) Electrical Processes in Atmospheres, 1-17, 10.1007/978-3-642-85294-7_1, 1976.

Motos, G., Corbin, J. C., Schmale, J., Modini, R. L., Bertò, M., Kupiszewski, P., Baltensperger, U., and Gysel-Beer, M.: Black Carbon Aerosols in the Lower Free Troposphere are Heavily Coated in Summer but Largely Uncoated in Winter at Jungfraujoch in the Swiss Alps, Geophysical Research Letters, 47, e2020GL088011, 10.1029/2020GL088011, 2020.

905   Nieminen, T., Kerminen, V. M., Petäjä, T., Aalto, P. P., Arshinov, M., Asmi, E., Baltensperger, U., Beddows, D. C. S., Beukes, J. P., Collins, D., Ding, A., Harrison, R. M., Henzing, B., Hooda, R., Hu, M., Hõrrak, U., Kivekäs, N., Komsaare, K., Krejci, R., Kristensson, A., Laakso, L., Laaksonen, A., Leaitch, W. R., Lihavainen, H., Mihalopoulos, N., Németh, Z., Nie, W., O'Dowd, C., Salma, I., Sellegri, K., Svenningsson, B., Swietlicki, E., Tunved, P., Ulevicius, V., Vakkari, V., Vana, M., Wiedensohler, A., Wu, Z., Virtanen, A., and Kulmala, M.:
910   Global analysis of continental boundary layer new particle formation based on long-term measurements, Atmos. Chem. Phys., 18, 14737-14756, 10.5194/acp-18-14737-2018, 2018.

Olin, M., Okuljar, M., Rissanen, M. P., Kalliokoski, J., Shen, J., Dada, L., Lampimäki, M., Wu, Y., Lohila, A., Duplissy, J., Sipilä, M., Petäjä, T., Kulmala, M., and Dal Maso, M.: Measurement report: Atmospheric new particle formation in a coastal agricultural site explained with binPMF analysis of nitrate CI-APi-TOF spectra,
915   Atmos. Chem. Phys., 22, 8097-8115, 10.5194/acp-22-8097-2022, 2022.

Pedersen, J., Nyord, T., Feilberg, A., and Labouriau, R.: Analysis of the effect of air temperature on ammonia emission from band application of slurry, Environmental Pollution, 282, 117055, 10.1016/j.envpol.2021.117055, 2021.

Petäjä, T., Mauldin Iii, R., Kosciuch, E., McGrath, J., Nieminen, T., Paasonen, P., Boy, M., Adamov, A., Kotiaho,
920   T., and Kulmala, M.: Sulfuric acid and OH concentrations in a boreal forest site, Atmos. Chem. Phys., 9, 7435-7448, 10.5194/acp-9-7435-2009, 2009.

Reche, C., Pérez, N., Alastuey, A., Cots, N., Pérez, E., and Querol, X.: 2011–2020 trends of urban and regional ammonia in and around Barcelona, NE Spain, Chemosphere, 304, 135347, 10.1016/j.chemosphere.2022.135347, 2022.

925   Reche, C., Querol, X., Alastuey, A., Viana, M., Pey, J., Moreno, T., Rodríguez, S., González, Y., Fernández-Camacho, R., de la Rosa, J., Dall'Osto, M., Prévôt, A. S. H., Hueglin, C., Harrison, R. M., and Quincey, P.: New considerations for PM, Black Carbon and particle number concentration for air quality monitoring across different European cities, Atmos. Chem. Phys., 11, 6207-6227, 10.5194/acp-11-6207-2011, 2011.

Reidy, B., Rhim, B., and Menzi, H.: A new Swiss inventory of ammonia emissions from agriculture based on a
930   survey on farm and manure management and farm-specific model calculations, Atmospheric Environment, 42, 3266-3276, 10.1016/j.atmosenv.2007.04.036, 2008.

Rinne, J., Ruuskanen, T. M., Reissell, A., Taipale, R., Hakola, H., and Kulmala, M.: On-line PTR-MS measurements of atmospheric concentrations of volatile organic compounds in a European boreal forest ecosystem, Boreal Environment Research, 10, 425-436, 2005.

935   Rivas, I., Beddows, D. C. S., Amato, F., Green, D. C., Järvi, L., Hueglin, C., Reche, C., Timonen, H., Fuller, G. W., Niemi, J. V., Pérez, N., Aurela, M., Hopke, P. K., Alastuey, A., Kulmala, M., Harrison, R. M., Querol, X.,

and Kelly, F. J.: Source apportionment of particle number size distribution in urban background and traffic stations in four European cities, Environment International, 135, 105345, 10.1016/j.envint.2019.105345, 2020.

940 Rodríguez, S. and Cuevas, E.: The contributions of "minimum primary emissions" and "new particle formation enhancements" to the particle number concentration in urban air, Journal of Aerosol Science, 38, 1207-1219, 10.1016/j.jaerosci.2007.09.001, 2007.

Rönkkö, T., Kuuluvainen, H., Karjalainen, P., Keskinen, J., Hillamo, R., Niemi, J. V., Pirjola, L., Timonen, H. J., Saarikoski, S., Saukko, E., Jarvinen, A., Silvennoinen, H., Rostedt, A., Olin, M., Yli-Ojanpera, J., Nousiainen, P., Kousa, A., and Dal Maso, M.: Traffic is a major source of atmospheric nanocluster aerosol, Proceedings of the
945 National Academy of Sciences of the United States of America, 114, 7549-7554, 10.1073/pnas.1700830114, 2017.

Saarikoski, S., Hellén, H., Praplan, A. P., Schallhart, S., Clusius, P., Niemi, J. V., Kousa, A., Tykkä, T., Kouznetsov, R., Aurela, M., Salo, L., Rönkkö, T., Barreira, L. M. F., Pirjola, L., and Timonen, H.: Characterization of volatile organic compounds and submicron organic aerosol in a traffic environment, Atmos.
950 Chem. Phys., 23, 2963-2982, 10.5194/acp-23-2963-2023, 2023.

Sánchez, G., Serrano, A., and Cancillo, M.: Effect of cloudiness on solar global, solar diffuse and terrestrial downward radiation at Badajoz (Southwestern Spain), Optica pura y aplicada, 45, 33-38, 2012.

Schraufnagel, D. E.: The health effects of ultrafine particles, Experimental & Molecular Medicine, 52, 311-317, 10.1038/s12276-020-0403-3, 2020.

955 Schultz, M. G., Schröder, S., Lyapina, O., Cooper, O. R., Galbally, I., Petropavlovskikh, I., von Schneidemesser, E., Tanimoto, H., Elshorbany, Y., Naja, M., Seguel, R. J., Dauert, U., Eckhardt, P., Feigenspan, S., Fiebig, M., Hjellbrekke, A.-G., Hong, Y.-D., Kjeld, P. C., Koide, H., Lear, G., Tarasick, D., Ueno, M., Wallasch, M., Baumgardner, D., Chuang, M.-T., Gillett, R., Lee, M., Molloy, S., Moolla, R., Wang, T., Sharps, K., Adame, J. A., Ancellet, G., Apadula, F., Artaxo, P., Barlasina, M. E., Bogucka, M., Bonasoni, P., Chang, L., Colomb, A.,
960 Cuevas-Agulló, E., Cupeiro, M., Degorska, A., Ding, A., Fröhlich, M., Frolova, M., Gadhavi, H., Gheusi, F., Gilge, S., Gonzalez, M. Y., Gros, V., Hamad, S. H., Helmig, D., Henriques, D., Hermansen, O., Holla, R., Hueber, J., Im, U., Jaffe, D. A., Komala, N., Kubistin, D., Lam, K.-S., Laurila, T., Lee, H., Levy, I., Mazzoleni, C., Mazzoleni, L. R., McClure-Begley, A., Mohamad, M., Murovec, M., Navarro-Comas, M., Nicodim, F., Parrish, D., Read, K. A., Reid, N., Ries, L., Saxena, P., Schwab, J. J., Scorgie, Y., Senik, I., Simmonds, P., Sinha, V.,
965 Skorokhod, A. I., Spain, G., Spangl, W., Spoor, R., Springston, S. R., Steer, K., Steinbacher, M., Suharguniyawan, E., Torre, P., Trickl, T., Weili, L., Weller, R., Xiaobin, X., Xue, L., and Zhiqiang, M.: Tropospheric Ozone Assessment Report: Database and metrics data of global surface ozone observations, Elementa: Science of the Anthropocene, 5, 10.1525/elementa.244, 2017.

Seinfeld, J. H. and Pandis, S. N.: Atmospheric chemistry and physics: from air pollution to climate change, John
970 Wiley & Sons, 2012.

Sun, J., Hermann, M., Weinhold, K., Merkel, M., Birmili, W., Yang, Y., Tuch, T., Flentje, H., Briel, B., Ries, L., Couret, C., Elsasser, M., Sohmer, R., Wirtz, K., Meinhardt, F., Schütze, M., Bath, O., Hellack, B., Kerminen, V. M., Kulmala, M., Ma, N., and Wiedensohler, A.: Measurement report: Contribution of atmospheric new particle formation to ultrafine particle concentration, cloud condensation nuclei, and radiative forcing – results from 5-
975 year observations in central Europe, Atmos. Chem. Phys., 24, 10667-10687, 10.5194/acp-24-10667-2024, 2024.

Tørseth, K., Aas, W., and Solberg, S.: The European Monitoring and Evaluation Programme (EMEP) – A Coordinated Effort to Provide Harmonized Observation of Air Pollution and Atmospheric Composition, in: Handbook of Air Quality and Climate Change, edited by: Akimoto, H., and Tanimoto, H., Springer Nature Singapore, Singapore, 149-156, 10.1007/978-981-15-2760-9_10, 2023.

980 Trechera, P., Garcia-Marlès, M., Liu, X., Reche, C., Pérez, N., Savadkoohi, M., Beddows, D., Salma, I., Vörösmarty, M., Casans, A., Casquero-Vera, J. A., Hueglin, C., Marchand, N., Chazeau, B., Gille, G., Kalkavouras, P., Mihalopoulos, N., Ondracek, J., Zikova, N., Niemi, J. V., Manninen, H. E., Green, D. C., Tremper, A. H., Norman, M., Vratolis, S., Eleftheriadis, K., Gómez-Moreno, F. J., Alonso-Blanco, E., Gerwig, H., Wiedensohler, A., Weinhold, K., Merkel, M., Bastian, S., Petit, J.-E., Favez, O., Crumeyrolle, S., Ferlay, N.,
985 Martins Dos Santos, S., Putaud, J.-P., Timonen, H., Lampilahti, J., Asbach, C., Wolf, C., Kaminski, H., Altug, H., Hoffmann, B., Rich, D. Q., Pandolfi, M., Harrison, R. M., Hopke, P. K., Petäjä, T., Alastuey, A., and Querol, X.:

Phenomenology of ultrafine particle concentrations and size distribution across urban Europe, Environment International, 172, 107744, 10.1016/j.envint.2023.107744, 2023.

990   Bundesamt für Umwelt: Luftqualität 2022: Messresultate des Nationalen Beobachtungsnetzes für Luftfremdstoffe (NABEL): https://www.bafu.admin.ch/bafu/de/home/themen/luft/publikationen-studien/publikationen/nabel-luftqualitaet.html, 2023.

Vana, M., Komsaare, K., Horrak, U., Mirme, S., Nieminen, T., Kontkanen, J., Manninen, H. E., Petaja, T., Noe, S. M., and Kulmala, M.: Characteristics of new-particle formation at three SMEAR stations, Boreal Environment Research, 21, 345-362, 2016.

995   Vestreng, V., Myhre, G., Fagerli, H., Reis, S., and Tarrasón, L.: Twenty-five years of continuous sulphur dioxide emission reduction in Europe, Atmos. Chem. Phys., 7, 3663-3681, 10.5194/acp-7-3663-2007, 2007.

Wang, J., Wu, Y., Ge, X., Shen, Y., Ge, S., and Chen, M.: Characteristics and sources of ambient refractory black carbon aerosols: Insights from soot particle aerosol mass spectrometer, Atmospheric Environment, 185, 147-152, 10.1016/j.atmosenv.2018.05.011, 2018.

1000   Xiao, M., Hoyle, C. R., Dada, L., Stolzenburg, D., Kürten, A., Wang, M., Lamkaddam, H., Garmash, O., Mentler, B., Molteni, U., Baccarini, A., Simon, M., He, X. C., Lehtipalo, K., Ahonen, L. R., Baalbaki, R., Bauer, P. S., Beck, L., Bell, D., Bianchi, F., Brilke, S., Chen, D., Chiu, R., Dias, A., Duplissy, J., Finkenzeller, H., Gordon, H., Hofbauer, V., Kim, C., Koenig, T. K., Lampilahti, J., Lee, C. P., Li, Z., Mai, H., Makhmutov, V., Manninen, H. E., Marten, R., Mathot, S., Mauldin, R. L., Nie, W., Onnela, A., Partoll, E., Petäjä, T., Pfeifer, J., Pospisilova, V.,
1005   Quéléver, L. L. J., Rissanen, M., Schobesberger, S., Schuchmann, S., Stozhkov, Y., Tauber, C., Tham, Y. J., Tomé, A., Vazquez-Pufleau, M., Wagner, A. C., Wagner, R., Wang, Y., Weitz, L., Wimmer, D., Wu, Y., Yan, C., Ye, P., Ye, Q., Zha, Q., Zhou, X., Amorim, A., Carslaw, K., Curtius, J., Hansel, A., Volkamer, R., Winkler, P. M., Flagan, R. C., Kulmala, M., Worsnop, D. R., Kirkby, J., Donahue, N. M., Baltensperger, U., El Haddad, I., and Dommen, J.: The driving factors of new particle formation and growth in the polluted boundary layer, Atmos.
1010   Chem. Phys., 21, 14275-14291, 10.5194/acp-21-14275-2021, 2021.

Yao, L., Garmash, O., Bianchi, F., Zheng, J., Yan, C., Kontkanen, J., Junninen, H., Mazon, S. B., Ehn, M., Paasonen, P., Sipila, M., Wang, M. Y., Wang, X. K., Xiao, S., Chen, H. F., Lu, Y. Q., Zhang, B. W., Wang, D. F., Fu, Q. Y., Geng, F. H., Li, L., Wang, H. L., Qiao, L. P., Yang, X., Chen, J. M., Kerminen, V. M., Petaja, T., Worsnop, D. R., Kulmala, M., and Wang, L.: Atmospheric new particle formation from sulfuric acid and amines
1015   in a Chinese megacity, Science, 361, 278-281, 10.1126/science.aao4839, 2018.

Yli-Juuti, T., Nieminen, T., Hirsikko, A., Aalto, P. P., Asmi, E., Hõrrak, U., Manninen, H. E., Patokoski, J., Dal Maso, M., Petäjä, T., Rinne, J., Kulmala, M., and Riipinen, I.: Growth rates of nucleation mode particles in Hyytiälä during 2003−2009: variation with particle size, season, data analysis method and ambient conditions, Atmos. Chem. Phys., 11, 12865-12886, 10.5194/acp-11-12865-2011, 2011.

1020   Yook, S. and Pui, D.: Estimation of penetration efficiencies through nasa sampling lines, submitted to C.-M. Lee, NASA Glenn Research Center, 2005.

Zanatta, M., Gysel, M., Bukowiecki, N., Muller, T., Weingartner, E., Areskoug, H., Fiebig, M., Yttri, K. E., Mihalopoulos, N., Kouvarakis, G., Beddows, D., Harrison, R. M., Cavalli, F., Putaud, J. P., Spindler, G., Wiedensohler, A., Alastuey, A., Pandolfi, M., Sellegri, K., Swietlicki, E., Jaffrezo, J. L., Baltensperger, U., and
1025   Laj, P.: A European aerosol phenomenology-5: Climatology of black carbon optical properties at 9 regional background sites across Europe, Atmospheric Environment, 145, 346-364, 10.1016/j.atmosenv.2016.09.035, 2016.

Zhou, Y., Hakala, S., Yan, C., Gao, Y., Yao, X. H., Chu, B. W., Chan, T., Kangasluoma, J., Gani, S., Kontkanen, J., Paasonen, P., Liu, Y. C., Petäjä, T., Kulmala, M., and Dada, L.: Measurement report: New particle formation
1030   characteristics at an urban and a mountain station in northern China, Atmos Chem Phys, 21, 17885-17906, 10.5194/acp-21-17885-2021, 2021.

Zhou, Y., Dada, L., Liu, Y., Fu, Y., Kangasluoma, J., Chan, T., Yan, C., Chu, B., Daellenbach, K. R., Bianchi, F., Kokkonen, T. V., Liu, Y., Kujansuu, J., Kerminen, V. M., Petäjä, T., Wang, L., Jiang, J., and Kulmala, M.: Variation of size-segregated particle number concentrations in wintertime Beijing, Atmos. Chem. Phys., 20, 1201-
1035   1216, 10.5194/acp-20-1201-2020, 2020.

Zhu, S., Yan, C., Zheng, J., Chen, C., Ning, H., Yang, D., Wang, M., Ma, Y., Zhan, J., Hua, C., Yin, R., Li, Y., Liu, Y., Jiang, J., Yao, L., Wang, L., Kulmala, M., and Worsnop, D. R.: Observation and Source Apportionment of Atmospheric Alkaline Gases in Urban Beijing, Environmental Science & Technology, 56, 17545-17555, 10.1021/acs.est.2c03584, 2022.

1040   Zotter, P., Herich, H., Gysel, M., El-Haddad, I., Zhang, Y., Močnik, G., Hüglin, C., Baltensperger, U., Szidat, S., and Prévôt, A. S. H.: Evaluation of the absorption Ångström exponents for traffic and wood burning in the Aethalometer-based source apportionment using radiocarbon measurements of ambient aerosol, Atmos. Chem. Phys., 17, 4229-4249, 10.5194/acp-17-4229-2017, 2017.

       Zotter, P., Ciobanu, V. G., Zhang, Y. L., El-Haddad, I., Macchia, M., Daellenbach, K. R., Salazar, G. A., Huang,
1045   R. J., Wacker, L., Hueglin, C., Piazzalunga, A., Fermo, P., Schwikowski, M., Baltensperger, U., Szidat, S., and Prévôt, A. S. H.: Radiocarbon analysis of elemental and organic carbon in Switzerland during winter-smog episodes from 2008 to 2012 – Part 1: Source apportionment and spatial variability, Atmos. Chem. Phys., 14, 13551-13570, 10.5194/acp-14-13551-2014, 2014.